Observation of collective modes of excitations in math xmlns="http://www.w3.org/1998/Math/MathML">mmultiscripts>mi>Co/mi>mprescripts>/mprescripts>none>/none>mn>59/mn>/mmultiscripts>mo>,/mo>/math> math xmlns="http://www.w3.org/1998/Math/MathML">mmultiscripts>mi>Ni/mi>mprescripts>/mprescripts>none>/none>mn>59/mn>/mmultiscripts>mo>,/mo>mo> /mo>mtext>and/mtext>mo> /mo>mmultiscripts>mi>Co/mi>mprescripts>/mprescripts>none>/none>mn>61/mn>/mmultiscripts>/math> and the influence of the math xmlns="http://www.w3.org/1998/Math/MathML">msub>mi>g/mi>mrow>mn>9/mn>mo>//mo>mn>2/mn>/mrow>/msub>/math> orbital

Samuel Ajayi, Vandana Tripathi, E. Rubino, Soumik Bhattacharya, L. T. Baby, R. S. Lubna, C. Benetti, Catur Wibisono, MacMillan B. Wheeler, S. L. Tabor, Yutaka Utsuno, Noritaka Shimizu, and J. M. Allmond

Phys. Rev. C **109**, 014305 — Published 2 January 2024

DOI: 10.1103/PhysRevC.109.014305

Understanding Excitations in ^{59,61}Co, ^{59}Ni

Samuel Ajayi,[*] Vandana Tripathi,[†] E. Rubino, Soumik Bhattacharya, L. T. Baby,
R. S. Lubna, C. Benetti, Catur Wibisono, MacMillan B. Wheeler, and S. L. Tabor
Department of Physics, Florida State University, Tallahassee, Florida 32306, USA

Yutaka Utsuno
Advanced Science Research Center, Japan Atomic Energy Agency, Tokai, Ibaraki 319-1195, Japan and
Center for Nuclear Study, University of Tokyo, Hongo, Bunkyo-ku, Tokyo 113-0033, Japan

Noritaka Shimizu
Center for Computational Sciences, University of Tsukuba, 1-1-1 Tennodai, Tsukuba 305-8577, Japan

J. M. Allmond
Oak Ridge National Laboratory, Physics Division, TN 37831-6371, USA

(Dated: November 16, 2023)

High spin states in ^{59}Co ($Z = 27$), ^{59}Ni ($Z = 28$) and ^{61}Co have been populated by the fusion evaporation reactions, ^{48}Ti(^{14}C, p2n)^{59}Co, ^{48}Ti(^{14}C, 3n)^{59}Ni, and ^{50}Ti(^{14}C, p2n)^{61}Co. The 9 MV tandem accelerator at the John D Fox Laboratory, Florida State University (FSU) was used to accelerate the ^{14}C beam and the de-exciting γ rays were detected by the FSU detector array consisting of six High Purity Germanium (HPGe) clover detectors, and three single crystals. Directional correlation of the γ rays de-exciting oriented states (DCO ratios) and polarization asymmetry measurements helped to establish spin and parities of the excited states whenever possible. The level scheme of ^{59}Co has been expanded with the inclusion of positive parity states upto $31/2^+$ at around 11 MeV. The ^{59}Ni positive parity states known from previous study were verified with modifications to some of the spins and parities. On the other hand, the negative parity states were extended to 31/2 at an excitation energy of 12 MeV. No new transition was observed for ^{61}Co, but one of the major bands has been reassigned as consisting of positive parity states by reason of this study. Excitations observed within the $f_{7/2}$, $p_{3/2}$, $f_{5/2}$ and $p_{1/2}$ orbitals, and also across the $N = 40$ sub-shell closure into the $g_{9/2}$ orbital was established by comparison with large-scale shell model calculations for the three nuclei studied.

I. INTRODUCTION

There has been a lot of interest in the study of nuclei around mass number A $\approx$ 60 in recent years. For nuclei in this mass region, the protons and neutrons both lie in the fp shell, near the doubly magic, spherical nucleus ^{56}Ni which can act as a natural core for understanding excitations. ^{56}Ni has proton number and neutron number equal to 28 and therefore the nucleons fill up the $f_{7/2}$ orbital. Any addition or subtraction of nucleons to this spherical nucleus can have an effect on its structure, especially at higher excitation. Nuclei with valence nucleons in the $p_{3/2,1/2}$ and $f_{5/2}$ orbitals, above the $f_{7/2}$ orbital, have the possibility of getting excited into the $g_{9/2}$ orbital which has been known to bring about collectivity. The collective excitations that have been observed in this mass region consist of magnetic rotation in nearly spherical nuclei and also rotation due to a deformed nucleus. Therefore, nuclei in this region are perfect for the study of structural changes from spherical to deformed configurations as a function of energy and angular momentum.

Several studies have been performed to investigate the excited states in nuclei in the mass A $\approx$ 60 region. Above the Z = 28 shell closure, the excited superdeformed states of ^{59}Cu and ^{61}Cu nuclei (Z = 29) have elucidated the evolution of nuclear shapes from spherical to deformed based on the $\nu g_{9/2}$ orbital [1, 2]. Similarly, for nuclei with Z $\leq$ 28, the neutron $g_{9/2}$ induces deformation and the onset of collectivity as has been reported in a large number of nuclei in this mass region like $^{57-60}$Mn (Z = 25), ^{57}Fe, ^{59,60}Fe (Z = 26), ^{61}Co (Z = 27), and ^{58}Ni (Z = 28) [3–7]. Magnetic rotation bands which were first observed in the near-spherical Pb isotopes with A $\approx$ 200 [8, 9], have also been observed in lighter nuclei in the A$\approx$ 60 mass region, like ^{58}Fe, ^{61}Co, ^{62}Co, ^{60}Ni, ^{61}Ni, and ^{62}Cu [6, 10–15].

To explain the experimental observations in this mass region both microscopic and macroscopic model have been employed. Shell model calculations have been quite successful in reproducing the low spin states in these nuclei whereas the particle rotor model and the cranked Nilsson-Strutinsky calculations have been used to interpret the rotational bands in many cases. Zhao *et al.* used the self-consistent tilted axis cranking relativistic mean-field theory based on a point-coupling interaction to investigate magnetic rotation bands in ^{60}Ni [16] while the Skyrme Hartree-Fock calculations was been used to describe the rotational bands observed in ^{57}Co [17, 18].

---

[*] soa19@fsu.edu
[†] vtripath@fsu.edu

Ref. [19] described the tilted axis cranking covariant density functional theory and its application for the magnetic rotation and antimagnetic rotation phenomen in different mass regions, while the Ref [14] used the technique to investigate the rotational bands in ^{61}Ni. Afanasjev *et. al.* used the cranked relativistic mean field theory and the configuration-dependent cranked Nilsson-Strutinsky approach to study superdeformed and highly deformed rotational bands in the A = 60 mass region [20].

Magnetic dipole rotation observed in near spherical nuclei is usually characterized by bands of strong M1 transitions as opposed to the E2 transitions which indicate rotation due to deformation. This phenomenon can be explained using the shears mechanism, where there is a coupling and gradual alignment of the spin of the protons and neutrons making up the total angular momentum of the levels, with the proton and neutron spin vectors as two blades of a shear [21–23]. The cross-over E2 transitions in these bands are generally weak or sometimes not observed as documented in the previous studies on magnetic rotation [23, 24]. Magnetic transition probability, B(M1) is expected to decrease with an increase in the total angular momentum vector as the magnetic moment reduces with the closing of the shear blades.

The isotopes, ^{59,61}Co and ^{59}Ni, which are the focus of this study all have protons occupying the $f_{7/2}$ orbitals (completely filled for ^{59}Ni). The neutrons on the other hand lie in the $\mathrm{p}_{3/2,1/2}$ and $\mathrm{f}_{5/2}$ orbitals, above the $\mathrm{f}_{7/2}$ orbital, and have the possibility of getting excited into the $\mathrm{g}_{9/2}$ orbital. The implication of this is that positive parity states can be generated at high spins, and since no experimental study on ^{59,61}Co has reported this before, it will be interesting to probe these high-spin states to observe the possibility. Also, given that magnetic rotation has been reported in ^{61}Ni, it becomes necessary to investigate if it also exists in ^{59}Ni which is just 2 neutrons less. The high-spin excitations give the perfect opportunity to investigate the structural changes from spherical to nearly deformed or deformed nucleus because their valence neutrons lie between the spherical closed shell nuclei and the deformation driving $\mathrm{g}_{9/2}$ orbital. Prior investigations of ^{59}Co using fusion evaporation reactions have not particularly focused on studying such structural changes [25–27]. Previous studies of ^{59}Ni and ^{61}Co have however focused respectively on rotational bands and the role of the $\mathrm{g}_{9/2}$ orbital in the development of collectivity [6, 28]. The experimental results from the high spin excitations will serve as a good testing ground of large-scale shell model calculation in a valence space including the $\mathrm{g}_{9/2}$ and $\mathrm{d}_{5/2}$ orbitals.

II. EXPERIMENTAL DETAILS

Two fusion-evaporation reaction experiments were performed at the John D Fox Laboratory, Florida State University (FSU) to populate and study the nuclei of interest. The beam used for both experiments is a long lived radioactive ^{14}C beam which was accelerated to an energy of 43 MeV using the 9 MV tandem accelerator. The targets were thin unbacked foils of ^{48}Ti and ^{50}Ti with thickness around $500 \mu g/cm^2$, and highly enriched up to over 90% for the particular isotope. The reaction ^{48}Ti(^{14}C, p2n)^{59}Co populated the high spin states of ^{59}Co by the evaporation of a proton and two neutrons (p2n channel). High spin states of ^{59}Ni were also populated using the same target in the reaction ^{48}Ti(^{14}C, 3n)^{59}Ni by the evaporation of three neutrons from the compound nucleus (3n channel). The reaction ^{50}Ti(^{14}C, p2n)^{61}Co on the other hand, populated the high spin states of ^{61}Co by the evaporation of a proton and two neutrons from the compound nucleus formed (p2n channel).

The FSU γ-detector array consisting of six High Purity Germanium (HPGe) clover detectors, and three single crystal Germanium detectors was used for detecting the γ rays from the excited states of the three nuclei. Three HPGe clover detectors were coupled to Bismuth Germanium Oxide (BGO) shields, an inorganic scintillator detector, which allows for Compton suppression. The detectors in the array were placed at 90°, 45°, and 135° with respect to the beam axis. This made the calculation for the Directional Correlation of Oriented States (DCO Ratio) possible. The energy and efficiency calibrations of the germanium detector array were performed using known calibrated ^{152}Eu, ^{133}Ba, and short-lived ^{56}Co sources. The ^{56}Co source was made at FSU using a proton beam. The spectra from the non 90° detectors were corrected for Doppler shift using the β (v/c) value of recoiling nuclei and the detection angle. The PIXIE digital data acquisition system was used to record the signals from the detectors and digitize for further analysis. For this experiment, the data was collected with a multiplicity setting greater than or equal to a 2-fold γ coincidence.

III. ANALYSIS

The event mode data was built into γ - γ matrices using the Gnuscope software developed at FSU. This was used for γ - γ coincidence analysis to identify new γ rays in coincidence with previously known transitions, which was then used to build up the level scheme as will be discussed. Angle-dependent asymmetric matrices were also made for Directional Correlation of Oriented States (DCO Ratio) analysis. The DCO ratio (R_{DCO}) technique was used to determine the spin of transitions, which infers the spin change between the energy levels connected by the transition. This spin change by extension was used to assign the spin of the higher energy level between levels joined by the transition. This assumes that the spin of the lower energy level is already known.

Given that γ_1, γ_2 are two γ peaks in coincidence, and θ_1, θ_2 are the angles of their detection, 90° and 135° in

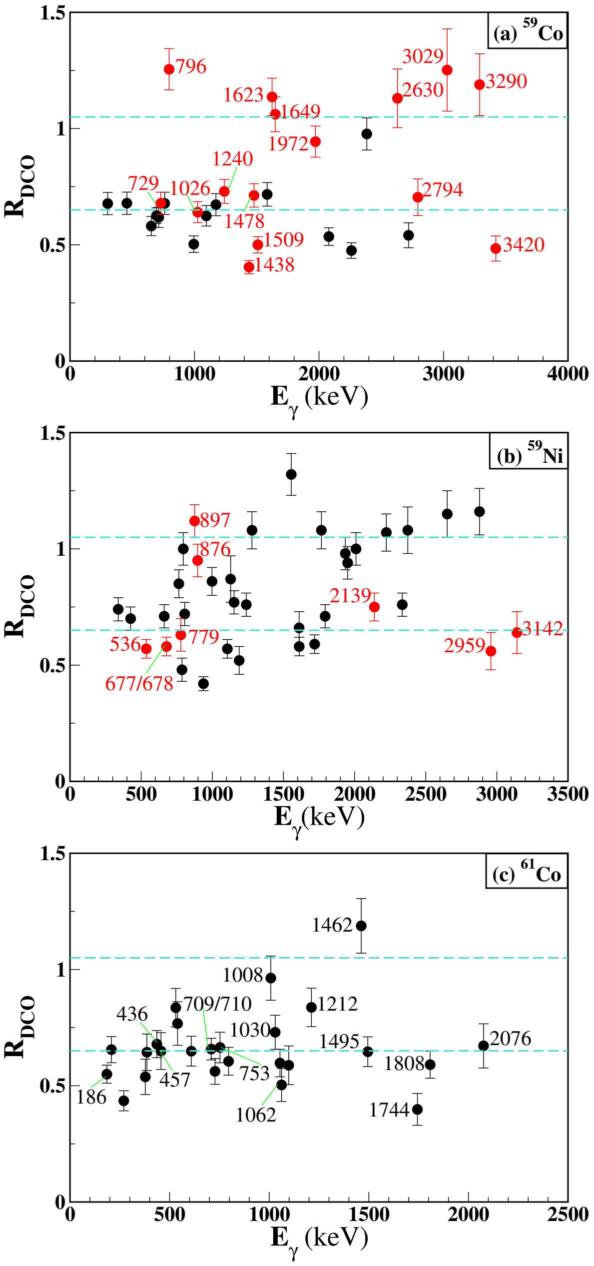

FIG. 1. (a) DCO ratio for transitions in ^{59}Co (b) DCO ratio for transitions in ^{59}Ni. For both (a) and (b) points labeled in red are newly placed while those labeled in black are known transitions (c) DCO ratio for transitions in ^{61}Co. All existing transitions are labeled in black. Point 709/710 represents the two transitions 709 keV and 710 keV which are both dipole in nature. For (a), (b), and (c), the transitions were from gates made on stretched quadrupole transitions.

our case, the R_{DCO} is given by [29]

$$R_{DCO} = \frac{I^{\gamma_2}_{\theta_1}(Gate^{\gamma_1}_{\theta_2})}{I^{\gamma_2}_{\theta_2}(Gate^{\gamma_1}_{\theta_1})} \tag{1}$$

where $I^{\gamma_2}_{\theta_1}(Gate^{\gamma_1}_{\theta_2})$ is the intensity of γ_2 determined from a spectrum in detectors at θ_1 gated on γ_1 detected by detectors at θ_2.

For gates that were made on pure dipole transitions, if the R_{DCO} is around 1 ± 0.3, then the transition is dipole and if R_{DCO} is around 1.85 ± 0.35, then it is a quadrupole transition. For gates that were made on pure quadrupole transitions, if R_{DCO} is around 0.55 ± 0.15, then the transition is dipole and if R_{DCO} is around 1.05 ± 0.25, then the transition is quadrupole. Figure 1 shows the plot of R_{DCO} with energy of γ transitions in ^{59}Co, ^{61}Co, and ^{59}Ni. The γ transitions with known multipolarities were in good agreement with our analysis giving us the confidence to make predictions for the new transitions.

Measuring the polarization asymmetry of the emitted γ rays helps in determining whether the γ ray transitions are magnetic or electric in nature. With this information, we can assign parity to the new states identified by the γ - γ coincidence analysis, having assigned spin values using the DCO ratio technique. The four crystals in the clover detectors located at 90° to the beam axis served as Compton Scattering polarimeter which makes polarization asymmetry measurements possible. The value of the polarization asymmetry A is positive for electric transitions and negative for magnetic transitions, and is given by [30]

$$A = \frac{aN_\perp - N_\parallel}{aN_\perp + N_\parallel} \tag{2}$$

$N_\perp$ and $N_\parallel$ are the numbers of γ rays Compton scattered in the perpendicular and parallel directions with respect to the beam axis. The factor, a is a correction term that is defined at A = 0 as

$$a = \frac{N_\parallel}{N_\perp} \tag{3}$$

The data was sorted into two hits for the clover detectors placed at 90° for polarization asymmetry; one parallel to the beam direction, and the other perpendicular to the beam direction. Using a ^{152}Eu unpolarized source, we measured the factor a, for different energy which was then fitted with a linear equation to obtain the factor a, as a function of energy. The uncertainty in the measured a is given by $\Delta a = 0.0600$, and it applies to the intercept of the equation (1.0372 ± 0.0600).

$$a = -3.05 \times 10^{-5} E_\gamma + 1.0372, \Delta a = 0.0600 \tag{4}$$

For all the γ transitions with good statistics, we calculated their polarization asymmetry as given in equations (2) and (4) and classified them as either electric or magnetic depending on the sign of A. The Figure 2 shows the polarization asymmetry of the γ transitions in the 3 nuclei, and their classification as either electric or magnetic is indicated.

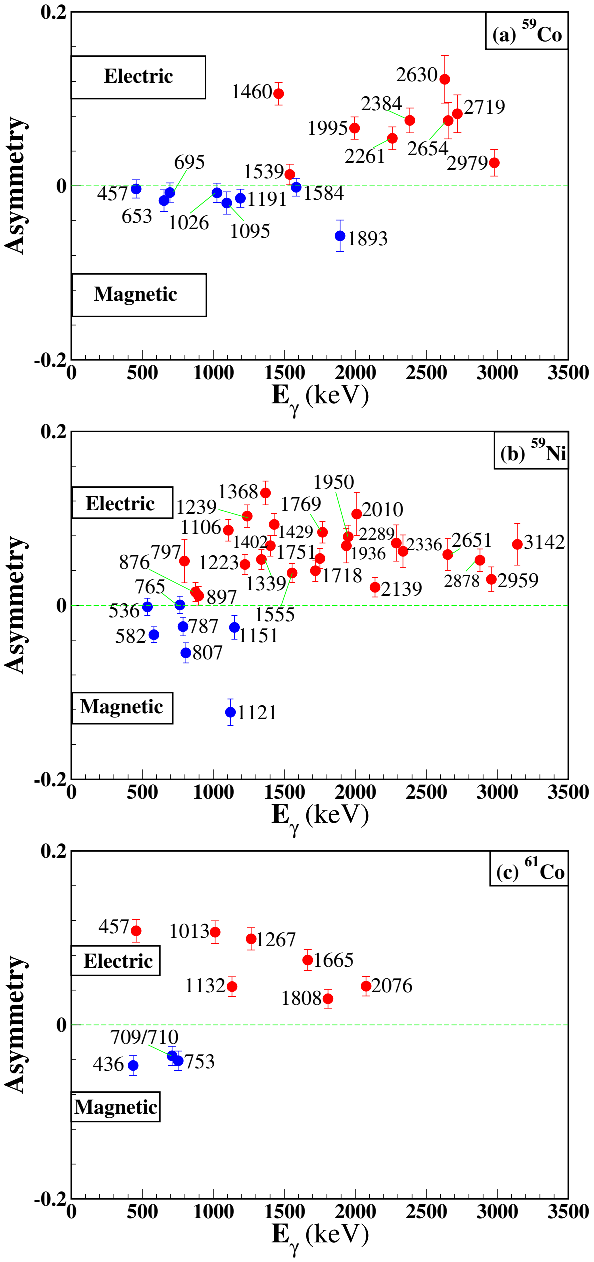

FIG. 2. The plot of polarization asymmetry vs. energy of γ-ray for (a) ^{59}Co, (b) ^{59}Ni and (c) ^{61}Co. Point 709/710 in (c) represents the two transitions 709 keV and 710 keV which are magnetic in nature. The points in red are electric transitions while the points in blue represent magnetic transitions.

IV. RESULTS

The combination of γ - γ coincidence analysis, R_{DCO} measurement, and polarization asymmetry measurements allowed us to build new expanded level schemes for the three nuclei in this study, ^{59}Co, ^{59}Ni, and ^{61}Co which will be discussed in the following sections.

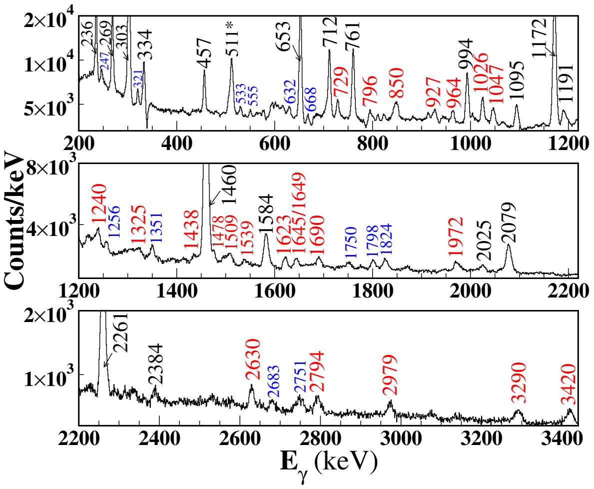

FIG. 3. 695-keV gate showing the γ ray energy peaks in ^{59}Co coincident with it. All the peaks labeled in red were newly discovered in this study. The 511-keV peak due to pair production is also shown; differentiated from other peaks with the * sign. The peaks labeled in blue are from possible contaminants from other nuclei also produced in the reaction; mostly from ^{58}Ni, ^{56}Fe, and ^{53}Cr.

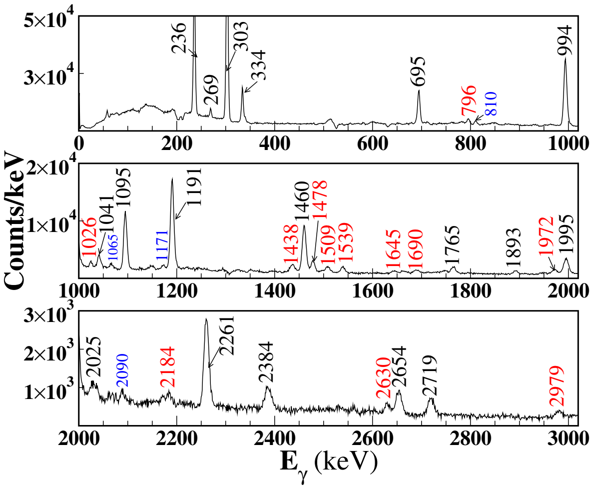

FIG. 4. 653-keV gate showing the γ ray energy peaks in ^{59}Co coincident with it. All the peaks labeled in red were newly discovered in this study. The peaks labeled in blue are from possible contaminants from other nuclei also produced in the reaction; mostly from ^{56}Fe and ^{58}Ni.

A. Level Scheme of ^{59}Co

In a previous study by Warburton *et al.* [25] using the ^{48}Ca(^{14}N, 3n)^{59}Co reaction, a maximum spin of 23/2 at an excitation energy of about 7.5 MeV was attained. In this current work, we have been able to confirm states predicted in the previous study and assigned parities to them. We have also extended the negative parity states to $27/2^-$ at around 9.6 MeV, while identifying positive parity states upto a $J^\pi = 31/2^+$ which had not been ob-

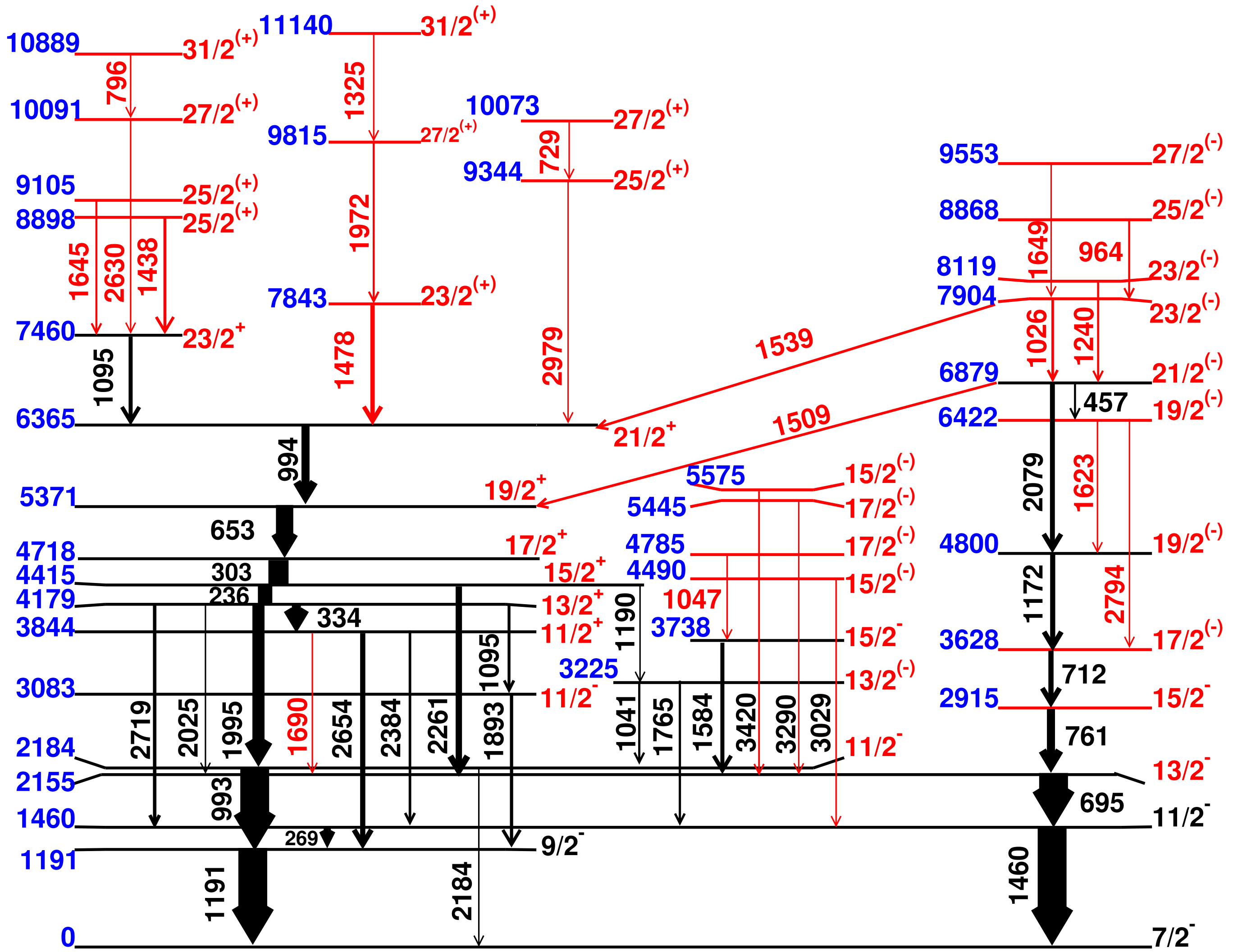

FIG. 5. Level scheme of ^{59}Co. All lines and labels in red are transitions and levels that were newly discovered in this study, while those in black have been discovered in previous studies. The thickness of the line arrows are approximately proportional to the intensity of the transitions. Spins and parities in parentheses are tentatively assigned based on expected patterns the level scheme since frequent parity change between consecutive levels is unlikely. The numbers in blue color are the energy level, distinguished from numbers in black which are the energies of the transitions.

served in any previous study of ^{59}Co. The multipolarity of the transitions in this study based on the value of the R_{DCO} and polarization asymmetry are given in Table I. Figures 1(a) and 2(a) display the numbers for ^{59}Co. The R_{DCO} value for the new transitions as seen in Figure 1(a) is based on the fact that the transition gated upon is a quadrupole transition.

Figures 3 and 4 show the coincident γ ray peaks when gates were defined on the 695-keV and the 653-keV transitions. These two gates show most of the transitions already known (labeled in black), and the new ones observed in this study (labeled in red). The peaks labeled in blue in the figures are mostly from other contaminants produced in this reaction. There are also a few peaks that might be in ^{59}Co but which we were unable to place in the level scheme. The expanded level scheme of ^{59}Co can be seen in Figure 5.

We have made an adjustment to two energy levels from the published level scheme in Ref [25]. The 3326-keV and 4087-keV levels have now been replaced with the 2915-keV and 3628-keV levels. This is driven by the fact that the observed intensities for the γ rays feeding the levels did not support the arrangement in the previous study. There are closeby 1168-keV and 1177-keV γ transitions observed in ^{56}Mn and ^{60}Co respectively, which influence the intensity of the 1172-keV γ transition observed in ^{59}Co. These nuclei are all produced in the reactions ^{14}C + ^{48}Ti (this current study) and ^{14}N + ^{48}Ca (previous study by study by Warburton *et al.* [25, 31]) according to PACE calculations [32, 33]. The intensity of the 1172-keV transition in ^{59}Co according to this study was used to determine its placement, and hence changed from where it was placed in the level scheme of Ref [25] as seen in Figure 5.

A major addition from the current work for ^{59}Co, is the identification of positive parity states which form a cascade. The transitions at 2654-, 1995- and 2261-keV were already known from previous studies and their placement could be verified in the current study. From the present R_{DCO} values these transitions were confirmed to be dipole transitions, but further, the polarization asymmetry measurements suggest that they are of electric nature, making them E1 transitions. This implies that they connect states with opposite parities. With the parities of the lower levels being negative we can conclude that the 2654-keV transition links the $11/2^+$ to the $9/2^-$ state, the 1995-keV transition links $13/2^+$ to $11/2^-$ state and the 2261-keV transition links the $15/2^+$ to the $13/2^-$ state. Beyond the $13/2^+$ state, a series of relatively strong M1 transitions were observed connecting the positive parity states with no measurable crossover E2 transitions. The multipolarities concluded for all the transitions based on R_{DCO} values and polarization asymmetry are listed in Table I with some plotted in Figures 1(a) and 2(a). Parities in parenthesis as seen in Table I and Figure 5 are tentatively assigned based on expected patterns of transitions between consecutive levels, knowing that a frequent parity change between the levels is unlikely.

In all, 22 new transitions were observed which resulted in 20 new energy levels. Nine of these new energy levels are of positive parity, in addition seven existing energy levels have now been identified as positive parity states.

B. Level Scheme of ^{59}Ni

In an earlier study by Juutinen *et al.* [34] in 1989, using the reaction ^{58}Ni(^{3}He, 2p)^{59}Ni, negative parity states were observed upto an excitation energy of 7.9 MeV with likely spin of $19/2^-$ or $21/2^-$. Positive parity states were also identified in the study, and the band built on the $9/2^+$ state at 3057 keV was expanded to an energy level of around 6 MeV, though definitive spin assignments were not made.

In a more recent study by Yu *et al.* [28], using the reaction ^{40}Ca(^{29}Si, 2α2p)^{59}Ni, four rotational bands were established with the highest spin observed to be 43/2. The two strongest bands (1 and 2 in Ref.[28]) are proposed to be generated by exciting one neutron and one neutron + one proton to the $g_{9/2}$ orbital respectively. They also indicated that the transition quadrupole moments of these bands decrease with spin suggestive of band termination.

In the present study, new transitions were established which were instrumental in the extension of the existing band of negative-parity states to around 12 MeV with spin $31/2^-$ which was earlier known only till 23/2 at an energy of 7954 keV from Ref. [34]. There is a new doublet of γ-ray transitions, 677-keV and 678-keV which appear in this band and can be seen in Figure 6 where the gate made on the 678-keV transition clearly shows the other peak measured as 677-keV. The intensity of the 677-keV implies the two transitions when arranged in the level scheme should be in close proximity. Figure 6 also shows some of the other new transitions: 779-keV, 1121-keV and 1918-keV associated with this band of negative parity states. There is also a connection observed to the $17/2^+$ state at 5255 keV via a new 1912-keV transition. Though this transition is close in value to other new transition, 1918-keV which exists in the band, the gate made on the 797-keV transition as seen in Figure 7 validates the placement of the 1912-keV transition. From the 807-keV gate shown in Figure 8, we could see some of the existing

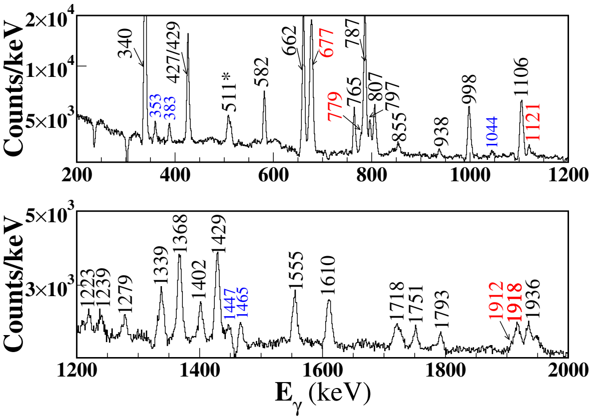

FIG. 6. Gate on 678-keV transition in ^{59}Ni. Another new 677-keV transition can be seen here. All the peaks labeled in red are some of the new transitions just observed in this study, including the 1918-keV transition. The 511-keV peak due to pair production is also shown; differentiated from other peaks with the * sign. The peaks labeled in blue are from possible contaminants from other nuclei also produced in the reaction; mo

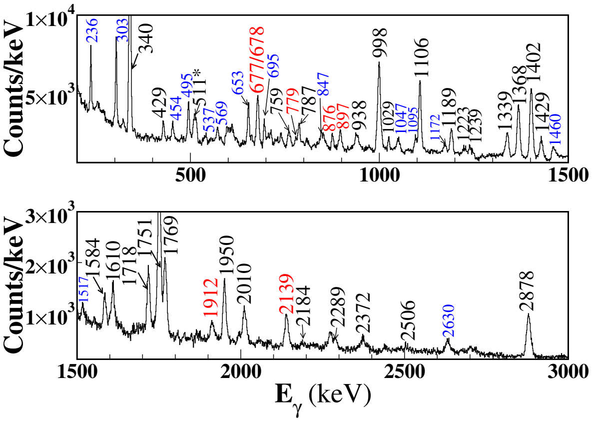

FIG. 7. Gate on 797-keV transition in ^{59}Ni. All the new transitions are labeled in red, including the 1912-keV transition. The 511-keV peak due to pair production is also shown; differentiated from other peaks with the * sign. The peaks labeled in blue are from possible contaminants from other nuclei also produced in the reaction; mostly from ^{59}Co, ^{58}Ni, and ^{60}Ni.

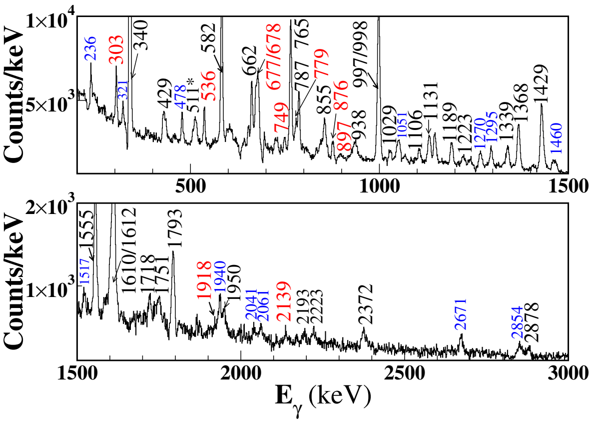

FIG. 8. Gate on 807-keV transition in ^{59}Ni. All the new transitions from the two negative bands show up here except for the 1918-keV transition. The 511-keV peak due to pair production is also shown; differentiated from other peaks with the * sign. The peaks labeled in blue are from possible contaminants from other nuclei also produced in the reaction; mostly from ^{58}Co, ^{60}Ni, ^{58}Ni, ^{59}Co, and ^{55}Fe.

transitions and some of the new transitions placed in the ^{59}Ni level scheme. The expanded level scheme of ^{59}Ni as a result of this work is shown in Figure 9 where red indicates new additions to the γ transitions.

A new sequence of negative-parity states is also proposed and built on the $17/2^{+}$ state at 5255 keV up to an energy of 9167 keV with a spin of 27/2. The new transition 2139 keV was clearly established to be an E1 transition according to Figures 1(b) and 2(b) and it connects the negative-parity state $19/2^{-}$ to the $17/2^{+}$ state. The 897-keV transition placed above the 2139-keV transition to link the $23/2^{-}$ to $19/2^{-}$ was further established as an E2 transition. We could not estimate the polarization asymmetry of the last transition 876-keV in the sequence though we could confirm it to be quadrupole in nature from the R_{DCO} value. Two new transitions were also added to the band of negative-parity states that terminated at 5.9 MeV in the previous study by Yu *et al.*, [28]. No spin or parity was assigned to the 5.9-MeV state then, but we have been able to assign a $17/2^{(-)}$ to it in this study. We assumed that the dipole transition 997 keV is most likely to be magnetic in nature, in line with the multipolarity of the 807-keV, 582-keV, and 536-keV transitions placed below and above it. The band was extended to 7.2-MeV at $21/2^{(-)}$ by the 536-keV and 749-keV transitions.

The sequence of positive parity states seen in the level scheme of ^{59}Ni (Figure 9) is analogous to band 1 and band 2 in Ref. [28] built on the $9/2^{+}$ state, though we found differences in some of the proposed spins and parities. The three transitions, 1106-keV, 1718-keV and 1751-keV had been identified as dipole transitions in previous studies. Based on our polarization asymmetry measurements we further confirmed them to be electric in nature and assigned them as E1 transitions. With that the spin-parities of the $9/2^{+}$ and $13/2^{+}$ are confirmed. Further up the 979-, 2878- and 1769-keV transitions build the band to $25/2^{+}$ at 9902 keV. We firmly established 2878 keV and 1769 keV as E2 transitions. Beyond that we see disagreements with the level structure proposed in Ref. [28]. In the gate of 1106 keV we could see the 1747 keV transitions and its R_{DCO} suggests it to be quadrupole and not dipole as in Ref. [28]. Similarly, the 2289-keV transition is established as a E2 transition opposite to Ref. [28] where it was thought to be an E1 transition though no polarization measurements are reported there. The R_{DCO} value for 2289-keV transitions was ascertained from two gates (both confirmed E2) namely 797 keV and 2878 keV making it a E2 transition. We further confirmed that the 2010-keV and 1223-keV transitions are E2 transitions. The 2372-keV transition was shown to be a quadrupole transition, though its asymmetry could not be ascertained. Using all this information, we established a sequence of E2 transitions connecting all positive parity states extending to 17.7 MeV with spin $41/2^{+}$. The multipolarities concluded for all the transitions based on R_{DCO} values and polarization asymmetry are listed in Table II. Parities (and spins) in parenthesis as seen in Table II and Figure 9 are tentatively assigned based on expected patterns of transitions between consecutive levels, and knowing that a frequent parity change between the levels is unlikely.

Overall, we observed 15 new transitions, and these in addition to some rearrangements brought about 14 new energy levels in the level scheme of ^{59}Ni.

C. Level Scheme of ^{61}Co

In a previous detailed study by Ayangeakaa *et al.* [6], the multinucleon transfer reaction, ^{26}Mg(^{48}Ca, $2\alpha4np\gamma$)^{61}Co in inverse kinematics was used to study the excited states of ^{61}Co. Six bands were identified as shown in the level scheme from that study, and all levels were assigned negative parity. In the current work, following the reaction ^{50}Ti(^{14}C, 2np)^{61}Co, we were able to observe five of the six bands previously identified. We were able to verify most of the transitions though we could not add any new γ-ray transitions. Figure 10 shows some of the transitions seen when a gate was made on the 1665-keV transition. Only two of the bands in this current study terminated on similar energy levels as in Ref. [6]. This is because of the higher γ-ray detection efficiency of Gammasphere used in Ref. [6] compared to the FSU γ array of primarily 6 clovers. Conversely the use of Clover detectors as Compton polarimeters in the current study allowed us to examine the parities of the levels. The level scheme as ascertained in this work is shown in Figure 11 where the bands are referred to as 1 to 5 going from left to right.

Consistent with the previous study, only in the fifth band starting with the $17/2^{-}$ state quadrupole transitions were observed connecting the exited states; all the

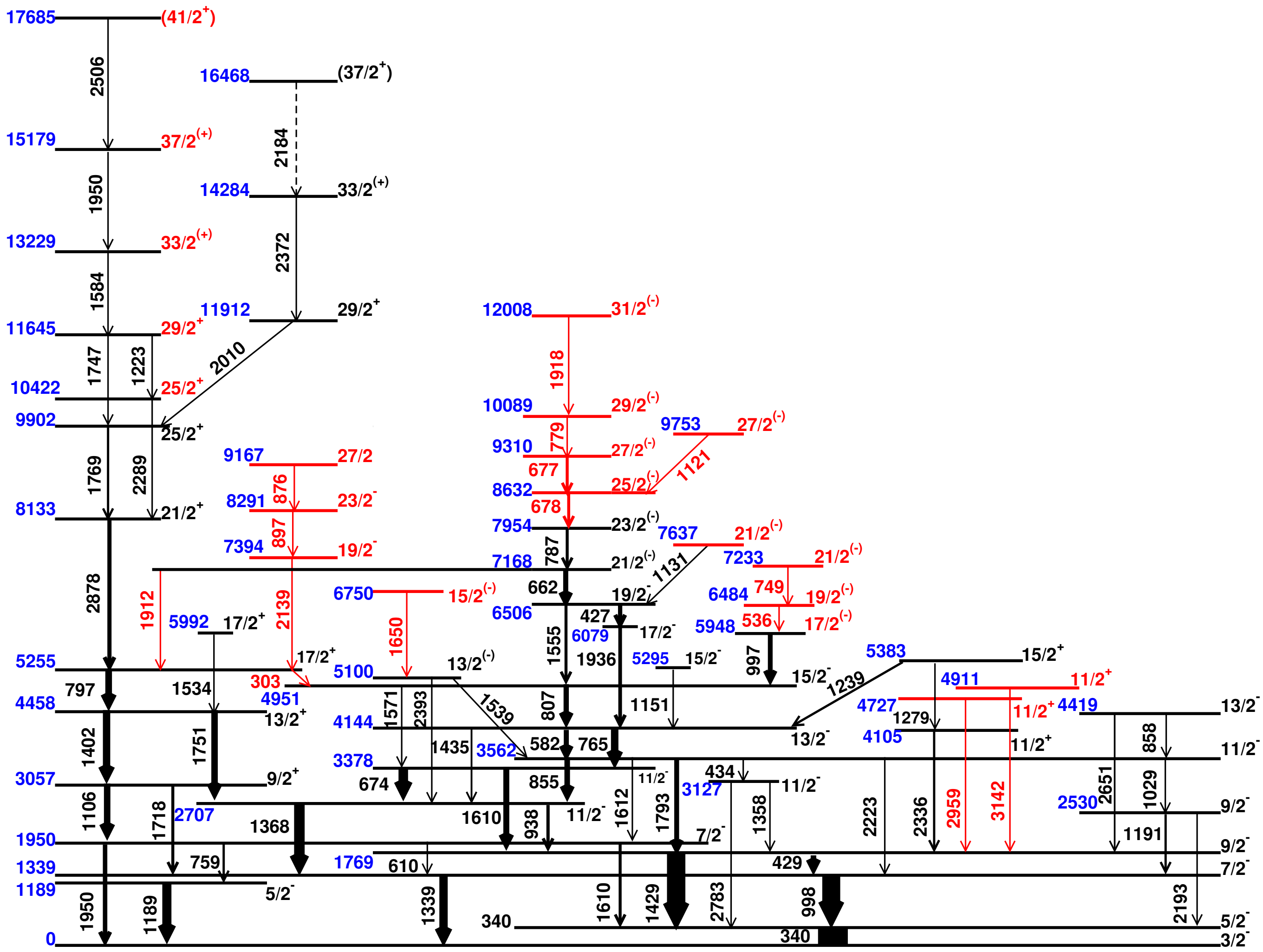

FIG. 9. Level scheme of ^{59}Ni showing the existing transitions and the new transitions observed in this study. All the energy levels in red are the newly established levels in this study. The thickness of the line arrows are approximately proportional to the intensity of the transitions. Spins and parities in parentheses are those tentatively assigned based on expected patterns the level scheme since frequent parity change between consecutive levels is unlikely. The numbers in blue color are the energy level, separated from numbers in black which are the energies of the transitions

other bands have a series of dipole transitions. We were able to clearly show that the 1267-keV has a E2 multipolarity, though for the 1008 keV we could only get a R_{DCO} value (Figure 1(c)) suggesting it to be quadrupole in nature. This band in Ref. [6] had 5 more transitions going upto a spin of 41/2 which we could not observe. But with the additional information from the current experiment, we can confirm that this band consists of E2 transitions.

As mentioned before, the inclusion of polarization measurements in this study to determine which transition is electric or magnetic in nature brought about a major change to the level scheme of ^{61}Co. The strong 1808-keV transition (see Fig. 10) connecting the states at 3473 keV and 1665 keV has now been confirmed to be dipole in nature as seen in the Figure 1(c). The polarization asymmetry measurement suggested that this transition is electric in nature as shown in Figure 2. This ascribes 1808-keV as an E1 transition which would link states of opposite parity. Hence it can be confirmed that the 1808-keV transition starts from a $13/2^+$ state at 3473 keV feeding the $11/2^-$ state at 1665 keV. The transition at 1132 keV was also confirmed to be dipole and electric in nature, thus making it an E1 transition. This served as an additional confirmation of the $13/2^+$ state in this study as it ends on the $11/2^-$ level. The 2076-keV transition which links bands 2 and 4 is also shown to be of E1 in nature, so we could firmly determine the 4094 level as positive parity. We adopted the parity assignment of the 6171-keV level from Ref [6] as negative. As for the 186-keV transition, we could only measure its R_{DCO} and not its polarization asymmetry, because being low in energy, the γ ray doesn't scatter, thereby making polarization measurement impossible. Even though we

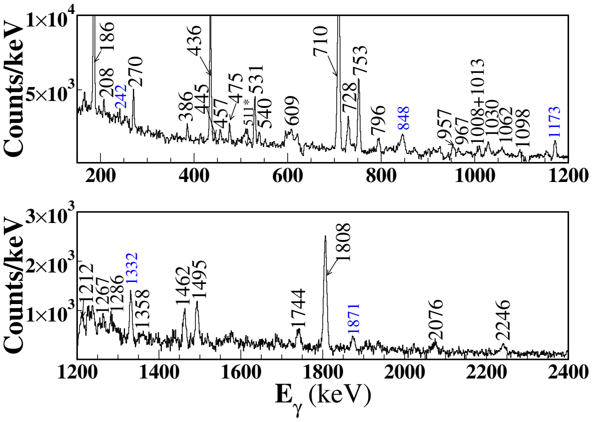

FIG. 10. Gate on the 1665-keV transition showing some of the already established transitions in ^{61}Co. No new transition was observed in this study, so all the peaks are labeled in black. The 511-keV peak due to pair production is also shown; differentiated from other peaks with the * sign. The peaks labeled in blue are from possible contaminants from other nuclei also produced in the reaction; mostly from ^{60}Ni.

only know the 186-keV transition is dipole in nature, we could indirectly infer its multipolarity, knowing that the 436-keV transition which is an M1 transition will link the $17/2^+$ state to the $15/2^+$ state at 3659-keV. With this information, we can state that the transitions above the 3473 keV level, namely 186-, 436- and 709 keV are M1 in nature. Beyond that, it was difficult to get both R_{DCO} and polarization asymmetry for all the transitions in the band because of low statistics and in the case of 1462 keV being a doublet. Details about the transitions, including their R_{DCO} values and polarization asymmetry are listed in Table III. In view of all the experimental observables from this work and Ref. [6], we can confidently state that band 2 starting at the $13/2^+$ state (3473 keV) is a sequence of M1 transitions connecting states with positive parity. It also agrees very well with shell model calculations as will be discussed next.

V. DISCUSSION

The odd-A nuclei studied in this work all have their valence nucleons occupying the *fp* shell according to the simple shell model picture. The Co isotopes, ^{59}Co and ^{61}Co have their unpaired 27^{th} proton in the $f_{7/2}$ orbital, leading to a ground state spin/parity of $7/2^-$. ^{59}Ni on the other hand has a closed shell for protons but its unpaired valence neutron lies in the $p_{3/2}$ orbital, so its ground state is $3/2^-$. Since the parity of the ground state energy level is negative, the confirmation of positive parity of some of the high spin states correspond to excitations across the $N = 40$ sub-shell closure into the positive parity $g_{9/2}$ orbital. The excitations into the $g_{9/2}$ orbitals can generate high spin and are also responsible for generating collective motion.

The shell model calculations to interpret the data were performed utilizing the M-scheme code KSHELL on the Oakbridge-CX supercomputer at the University of Tokyo [35]. Both negative and positive parity states were generated from the shell model calculation. The model space was taken as *fp* shell for the negative parity states and the GXPF1Br interaction was used for that. For the positive parity states however, the model space was taken as the *fp* shell, $0g_{9/2}$, and $1d_{5/2}$ orbits, restricting one neutron excitation to the $0g_{9/2}$, and $1d_{5/2}$ orbits. In addition, up to 6-particle 6-hole excitation from the $0f_{7/2}$ orbit is allowed for the case of ^{59}Ni and ^{59}Co. The GXPF1Br+V_{MU} interaction was used for the full calculation [36]. The predictions of the shell model calculation for the three nuclei in consideration align well with the experimental results. The root-mean-square (RMS) difference between the experimental results and the theoretical calculation averages below 200 keV. Table IV and Figures 12, 13, 14 show the comparison between the calculation and experiment. For the figures, the asterisks in red represent the experimental results and the squares in blue are the results from the shell model calculation for the yrast states. Figures 12 (a), 13 (a) and 14 (a) additionally include the yrare negative-parity states (*i.e.* 2nd excited state of each spin), with the experimental values represented by green circles, and the calculation represented by the green line. For the states where there are existing experimental values for the mean lifetime, we estimated the theoretical mean lifetime using the predicted $B(M1)$ values and found them to be in quite good agreement. The details of the calculations will be discussed in greater detail below, in relation to the experimental results for each nuclide.

A. ^{59}Co

^{59}Co has 27 protons and 32 neutrons, leading to all its valence nucleons in the *fp* shell. With 7 protons outside the closed *sd* shell at $Z = 20$, we expect an unpaired proton in the $0f_{7/2}$ orbit. The 12 neutrons on the other hand outside the closed sd shell are all paired and not contribute to the ground state spin value expected to be $7/2^-$ because of the unpaired proton. Of the 12 neutrons, 8 neutrons fill the $0f_{7/2}$ orbit, while the remaining 4 neutrons are expected to fill the $1p_{3/2}$ orbit. However, as $1p_{3/2}$ and $0f_{5/2}$ levels are close in energy, both levels share the 4 neutrons in the ground state as per the calculations performed. This ground state configuration is verified by picturing ^{60}Co as ^{59}Co + n in the ^{59}Co (d,p) reaction studied by Roy et. al., to produce ^{60}Co [37]. If the four neutrons outside the closed $0f_{7/2}$ shell filled up the $1p_{3/2}$ orbit, then the (d,p) reaction leading to the ground state of ^{60}Co should be characterised by an $\ell = 3$ transition (coming from the $0f_{5/2}$ level). But all (d,p) reactions leading to the ground state and the isomeric state at 60 keV have $\ell = 1$ (coming from the $1p_{3/2}$ level), therefore pointing to the fact that there is a vacancy in

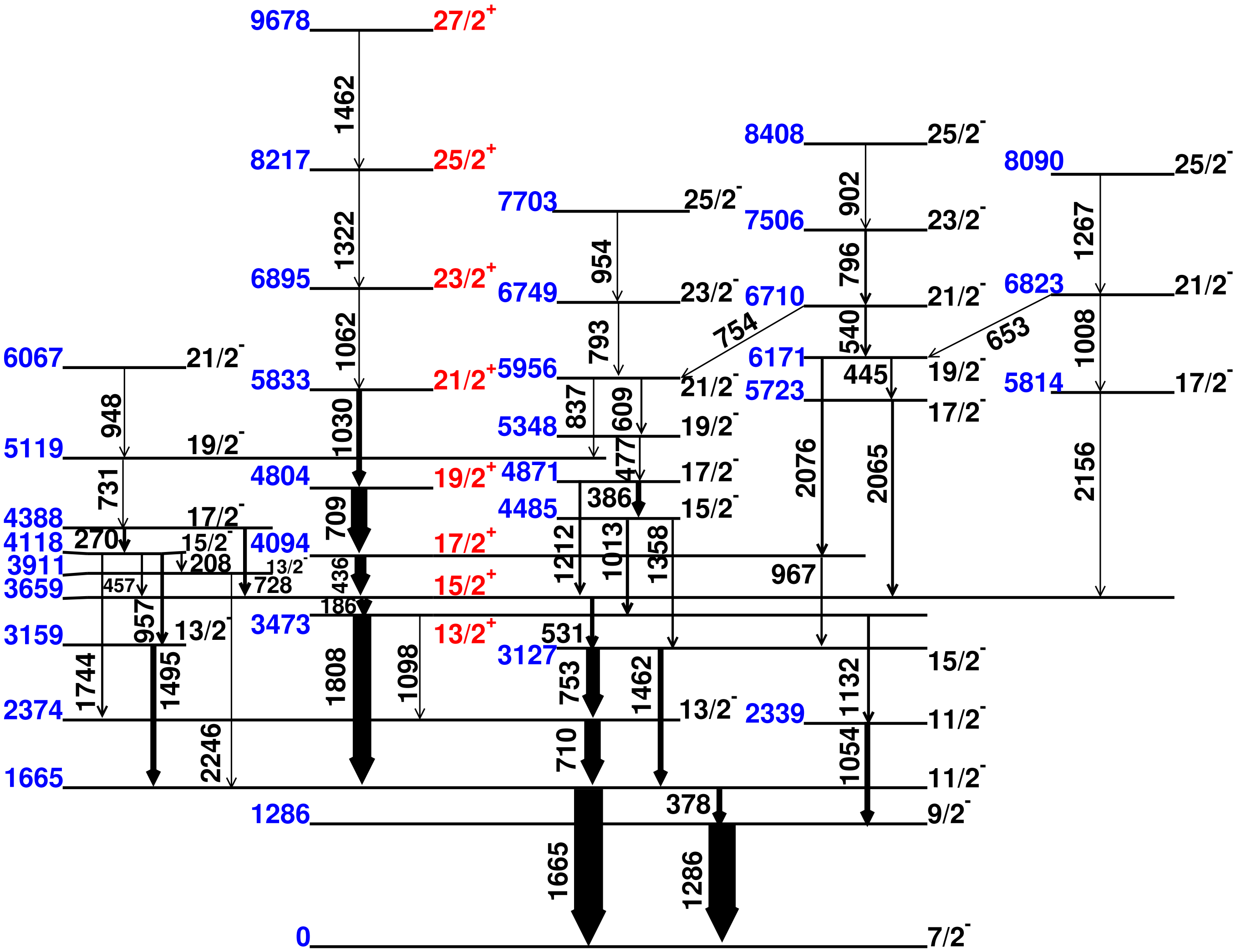

FIG. 11. Level scheme of ^{61}Co confirming the existing transitions and energy levels. The spin and parity shown in red are the new important features added to this level scheme. The thickness of the line arrows are approximately proportional to the intensity of the γ-ray transitions. The numbers in blue color are the energy level, separated from numbers in black which are the energies of the transitions

the $1p_{3/2}$ orbit in ^{59}Co to accommodate a neutron. We conclude therefore that in the ground state, ^{59}Co likely has 2 valence neutrons each in the $1p_{3/2}$ and $0f_{5/2}$ levels consistent with the shell model calculations.

The excitations at low spin to negative parity states are likely single-particle excitations within the fp shell, *i.e.* $0p0h$ excitations. The shell model calculations for the $0p0h$ negative-parity states align well with the experimental result up till the $27/2^-$ level as seen in Figure 12 and Table IV. The positive parity states arise from $1p1h$ excitations where a nucleon is excited to the $g_{9/2}$ orbit leaving an even number of neutrons in the fp shell. From Figure 12, we can see a good agreement between the shell model calculation and the experimental result. The $9/2^+$ state predicted by the calculation as the lowest positive parity state was not observed in the experiment because it is not yrast.

The positive parity states in ^{59}Co form a regular pattern with a series of M1 transitions from the $13/2^+$ state upwards to the $23/2^+$ state. Experimental values for the mean lifetime of the states $17/2^+$, $19/2^+$, and $21/2^+$ have been given by Ref [25] as 1.1(4) ps, 0.10(5) ps, and < 0.20 ps respectively. The B(M1) (down) from the shell model calculation for the respective states are 1.69 μ_N^2, 1.53 μ_N^2, and 1.30 μ_N^2, from which we obtained a theoretical mean lifetime of 1.21 ps, 0.13 ps, and 0.045 ps. The mean lifetime measurement from the experimental and theoretical approach seems to agree. Further, the $13/2^+$, $15/2^+$ and $23/2^+$ states in the band has B(M1) values of 0.28 μ_N^2, 1.54 μ_N^2, and 0.58 μ_N^2 respectively. It is observed that the reduced transition probability B(M1) became strong at $15/2^+$, reached a peak at $17/2^+$, and then started reducing gradually as spin increases. The highest B(M1) value here approaches the lower limit of 2 - 10 μ_N^2 which

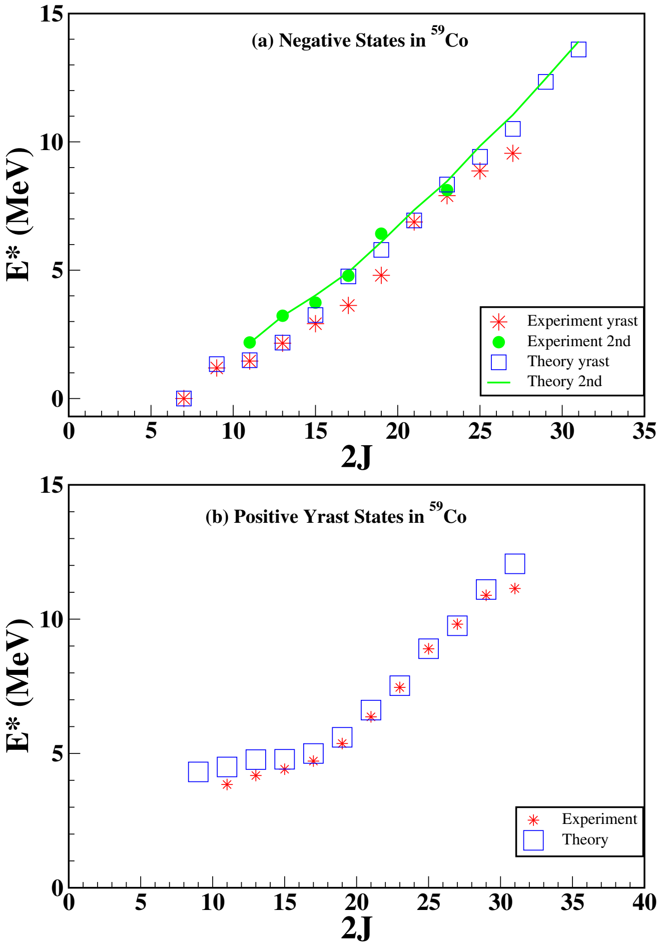

FIG. 12. Comparison of theoretical shell model calculation with experimental results in ^{59}Co. The red star symbol represents experimental values while the blue box symbol represents values from the theoretical shell model calculation. In (a), the “experiment 2nd” and the “theory 2nd” are the second states (near y-rast, also called yrare states), and are represented with green color; circles for experimental values, and line for the theoretical shell model calculation.

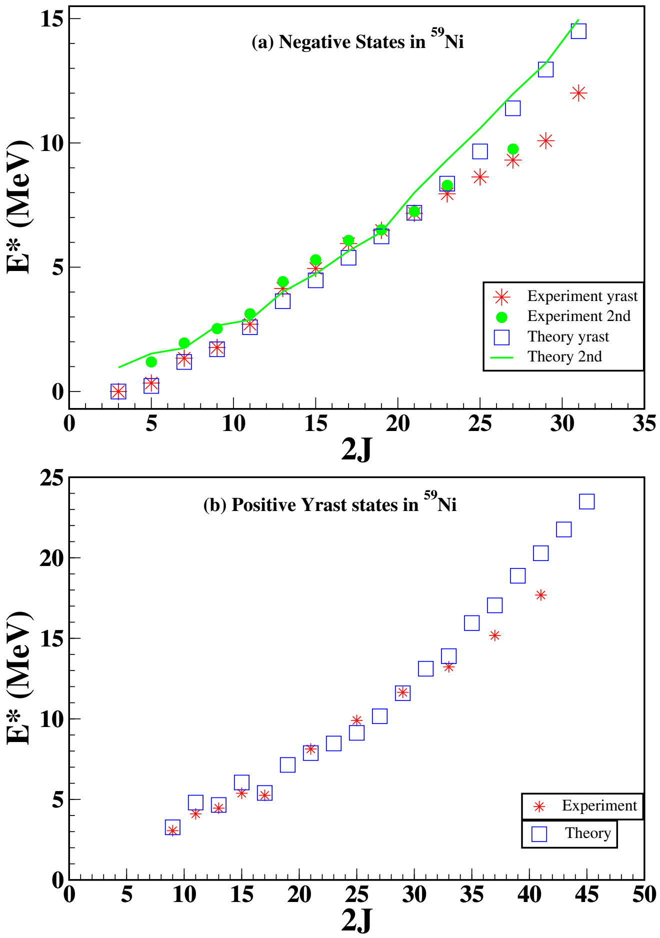

FIG. 13. Comparison of theoretical shell model calculation with experimental results in ^{59}Ni. The red star symbol represents experimental values while the blue box symbol represents values from the theoretical shell model calculation. In (a), the “experiment 2nd” and the “theory 2nd” are the second states (near y-rast, also called yrare states), and are represented with green color; circles for experimental values, and line for the theoretical shell model calculation.

has been observed for magnetic rotation bands in nuclei in higher mass region [24]. Overall, the patterns seen in this band till $23/2^+$ is indicative of what is expected of the magnetic transition probabilities for the magnetic rotation sequence [24].

The positive parity states in consideration can be viewed as part of collective excitation because of the regularity observed in the γ transitions linking the states. The presence of relatively strong M1 transitions points to the possibility of a magnetic rotation band. In magnetic transition bands, the magnetic transition probability, experimentally indicated by transition intensities is expected to decrease until the band terminates. The $g_{9/2}$ orbit involved in the formation of positive parity states allows high spin to be generated and also fulfills the neutron particle, proton hole coupling condition for magnetic rotation as explained by Clark, and Macchiavelli [24]. The dominant configuration for the band of positive parity states is $\pi(f^{-2}_{7/2}p^{1}_{3/2})\otimes\nu(p^{2}_{3/2}g^{1}_{9/2})$. The predicted occupancies of the states in this proposed magnetic rotation band according to the shell model calculation can be seen from Figure 15 (a) and highlight the very similar configuration for the whole band.

B. ^{59}Ni

^{59}Ni has a full $0f_{7/2}$ orbital for both protons and neutrons, leaving 3 extra neutrons to fill the $1p_{3/2}$ orbit. With this configuration, the spin-parity of the ground state is $3/2^-$ as a consequence of an unpaired neutron in the $1p_{3/2}$ orbit. The first excited state with $5/2^-$ can be generated by the unpaired neutron moving from the $1p_{3/2}$ orbital to the $0f_{5/2}$ and is seen experimentally at 340 keV.

The low-lying negative parity excited states have irregular energy transitions linking them that are suggestive of single-particle excitations within the *fp* shell. Other nuclei in this A = 60 mass region have been found to exhibit similar single particle excitation for the low-lying states [6, 13]. There is a good agreement between the shell model calculations for the negative parity states and experimental results up until the $23/2^-$ as seen in Figure 13 and Table IV. Comparing the B(E2) values from our shell model calculation to the available evaluated data for low lying states, it can be argued these states are non-collective in nature. Measured B(E2) values (in W.U) for the $7/2^-$, $7/2^-_2$, $9/2^-$ and $11/2^-$ states are given as 3.0(8), 12 (11), 10 (3) and 22 (5) respectively, while the theoretical calculations give 0.7, 16, 5.7 and 9.3 respectively. While there is a good agreement between the shell model calculations and the experimental results for the low lying states, we see a pronounced variation from the $25/2^-$ state and beyond. This discrepancy can be due to a different configuration for these high spin states likely involving more particles in the $g_{9/2}$ orbital. The excitation energy needed to generate these states in the collective model is likely lower than in the shell model picture.

The first excited positive parity state from the level scheme is a $9/2^+$ state and can be easily generated by having a neutron in the $g_{9/2}$ orbital while all the other nucleons are paired in the *fp* shell. The dominant configuration we, however, see from the theoretical prediction for the band of positive parity states is $\pi(f^{-1}_{7/2}p^1_{3/2})\otimes\nu(f^{-1}_{7/2}p^1_{3/2}f^1_{5/2}g^1_{9/2})$ (see Figure 15 (b) for the theoretical predictions). The shell model calculation for the yrast positive parity states aligns with the experimental results up till the $33/2^+$ state. Further up, starting from the $37/2^+$ state we again see a discrepancy between the shell model calculations and experimental results. This may also be due to a change in the configuration not captured by the shell model calculations as we move from the $33/2^+$ level to $37/2^+$. Such a change of configuration was also observed in rotational bands in the study of ^{61}Ni [13], where the two configurations were illustrated by two fits to the rotational model.

Among the positive parity states, there is a sequence of E2 transitions from $9/2^+$ to $41/2^+$ which may be a pointer to rotational motion. Given the different configurations in different spin regions across this positive band, there seem to be different possible deformation configurations in this band. Since it is the rotation of a deformed nucleus that gives rise to regular bands observed in the spectrum of nuclei [24], it suggests ^{59}Ni could be deformed at excitations involving the deformation driving $g_{9/2}$. Rotation has been established in the four bands observed in the study of ^{59}Ni by Yu *et al.* [28]. The more populated bands 1 and 2 in the study correspond to the bands of positive parity states in our study. Cranked Nilsson-Strutinsky (CNS) calculations [38] were performed in the study, and it indicated substantial collectivity in the band structures of ^{59}Ni. Similar deformed bands with a sequence of E2 transitions were also established in the neutron-rich ^{61}Ni by Bhattacharya *et al.* [13].

The negative parity high spin states from $19/2^-$ to $31/2^-$ show a sequence of M1 transitions connecting the states. This could be an indication of magnetic rotation as was observed in ^{59}Co. The configuration of these states could correspond to no valence nucleon in the $g_{9/2}$ orbit or 2 nucleons occupying the $g_{9/2}$ orbital. The dominant configuration of the $19/2^-$ state according to our shell model calculation which cannot account for 2 particle excitation is given by $\pi(f^{-2}_{7/2}\ p^1_{3/2})\otimes\nu(f^{-1}_{7/2}p^2_{3/2}\ f^2_{5/2})$. The excitation from the $f_{7/2}$ orbital into the higher orbitals within the *fp* shell could in principle generate proton and neutron angular momentum needed for magnetic rotation. Ref [39] indicated the possibility of magnetic rotation in the *sd*-shell region, where the highest available j orbital is $d_{5/2}$. This suggests there is a possibility for observing magnetic rotation without the inclusion of the $g_{9/2}$ orbital. The B(M1) for the states in consideration from the shell model calculations are all however less than 0.1 μ_N^2, which is small compared to the values for the M1 bands in ^{59}Co and ^{61}Co (to be discussed). Ref. [39] also hinted that low B(M1) values will likely result from the unavailability of high j orbitals involved in the angular momentum coupling.

The implication of this result is that there might be two modes of excitation in this nucleus competing; one driven by the deformation of the nucleus, and the other, probably magnetic rotation due to the angular momentum coupling of the protons and neutrons. Though this is not new as it has been noted earlier in Refs [6, 10, 12, 13] in their study of ^{61}Co, ^{58}Fe, ^{60}Ni, and ^{61}Ni, still it is interesting to see the extent of such a phenomenon with changing neutron numbers.

C. ^{61}Co

^{61}Co with 27 protons and 34 neutrons has a ground state spin-parity of $7/2^-$ just like ^{59}Co. It can be seen as ^{59}Co + 2n, so it is expected that excitations for the two isotopes have similarities. The first four excited states in the two nuclei are similar in energy levels. The first excited state, $9/2^-$ is at 1.19 MeV and 1.29 MeV in ^{59}Co and ^{61}Co respectively. The difference in the energies of the yrast states are 95 keV at $9/2^-$, 205 keV at $11/2^-$, 219 keV at $13/2^-$ and 211 keV at $15/2^-$. Therefore, it can be expected that the same pattern of excitation will follow at low spins before the additional neutron pair is broken, and its excitation contributes to the spin of the nucleus. These considerable similarities in the low-lying spins are in agreement with the conclusions of Ref. [26] on the similarities between the energy levels of the low-lying states of ^{57}Co, ^{59}Co and ^{61}Co.

The randomness of the transitions within the low-lying negative parity states in the level scheme suggests single particle excitation and seems to follow a 0*p*0*h* excitation

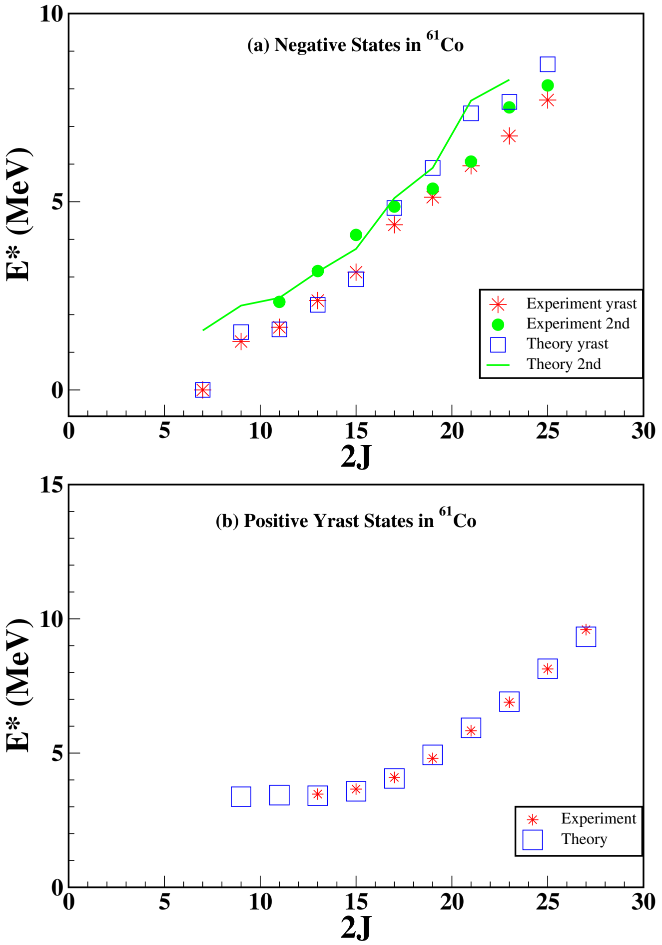

FIG. 14. Comparison of theoretical shell model calculation with experimental results in ^{61}Co. The red star symbol represents experimental values while the blue box symbol represents values from the theoretical shell model calculation. In (a), the “experiment 2nd” and the “theory 2nd” are the second states (near y-rast, also called yrare states), and are represented with green color; circles for experimental values, and line for the theoretical shell model calculation.

pattern. Figure 14 and Table IV shows the comparison between the shell model calculation and the experimental results. Overall, a good agreement is observed, except for negative parity states from around $21/2^-$ upwards, where there seems to be a departure between the calculation and the experiment. It can be seen from the level scheme that the high-lying negative parity states are all linked by transitions to the $13/2^+$, $15/2^+$ and $17/2^+$ states which are $1p1h$ excitation and hence they could possibly represent $2p2h$ excitations, with two nucleons residing in the $g_{9/2}$ orbit. Configurations involving two $g_{9/2}$ neutrons were also suggested by Ref [6] while discussing rotational bands in the high-lying negative parity states of ^{61}Co however such calculations are not currently possible.

The positive parity states assigned in this study of ^{61}Co are a natural extension of what we observed in ^{59}Co. In Ref. [6] these were not proposed as positive parity states as linear polarization measurement was not performed in that study. They did though observe a difference in the excitation pattern above 4 MeV, (which corresponds to $17/2^+$) and therefore suggested that the description of higher-lying states in ^{61}Co should be carried out in an expanded model space beyond the fp shell [6], which has been done in this current study to predict the positive parity states. From Figure 14, we see a good agreement between the shell model calculations for the positive parity states and the experimental results. The occupancies associated with the positive parity band are displayed in Figure 15 (c). The regularity observed in this band of positive parity states which contains a series of M1 transitions is again an indication of magnetic rotation. Experimental value for the “apparent” lifetime of the $17/2^+$ state has been measured by Ref [40] and Ref [41] as 1.1(0.3) ps. The B(M1) from the shell model calculation for the strongest transition from the $17/2^+$ state is 1.0 μ_N^2, from which we obtained a theoretical partial mean lifetime of 0.69 ps for the state. Converting this theoretical partial mean lifetime into total mean lifetime using the branching ratio from Table III gives a value of 0.57 ps. The “apparent” lifetime from Ref [40] represents an upper limit for the experimental mean lifetime of the state. The theoretical B(M1) values were obtained for other states, $15/2^+$, $19/2^+$, $21/2^+$, $23/2^+$ in the band and are 1.17 μ_N^2, 0.81 μ_N^2, 0.22 μ_N^2, and 0.5 μ_N^2 respectively. The values shows an approximate pattern expected of the magnetic transition probabilities (reduction) with spin increase as explained by Ref [24].

The dominant configuration for the band of positive parity states according to shell model calculation is $\pi(f^{-2}_{7/2}p^{1}_{3/2})\otimes\nu(p^{-1}_{3/2}f^{2}_{5/2}g^{1}_{9/2})$ (Figure 15 (c)). The other bands of high-lying negative parity states also have M1 transitions and could be candidates for magnetic rotation too. We also observe the established band of E2 transitions indicative of rotation due to deformation, but it terminates quickly in this study. Just as was discussed for ^{59}Ni, different modes of excitations are observed in the case of ^{61}Co. Ref [6] concluded that in ^{61}Co, quadrupole collectivity associated with a prolate shape competes for yrast status with the magnetic rotation of a nearly spherical system. Our results in general also support the notion that there is a competition between the magnetic rotation and the rotation due to deformation in this nucleus.

VI. SUMMARY

In the current work, we have studied the structure of three nuclei with $A \approx 60$; namely ^{59}Co, ^{59}Ni and ^{61}Co using a ^{14}C beam on ^{48}Ti and ^{50}Ti targets. The level scheme of ^{59}Co now includes positive parity states which has been extended to $31/2^+$ at around 11 MeV. The positive parity states in the ^{59}Ni level scheme are now extended to $41/2^+$ at excitation energy 17.7 MeV. The negative parity states have also been extended to $31/2^-$ at excitation energy of 12 MeV. There were no new tran-

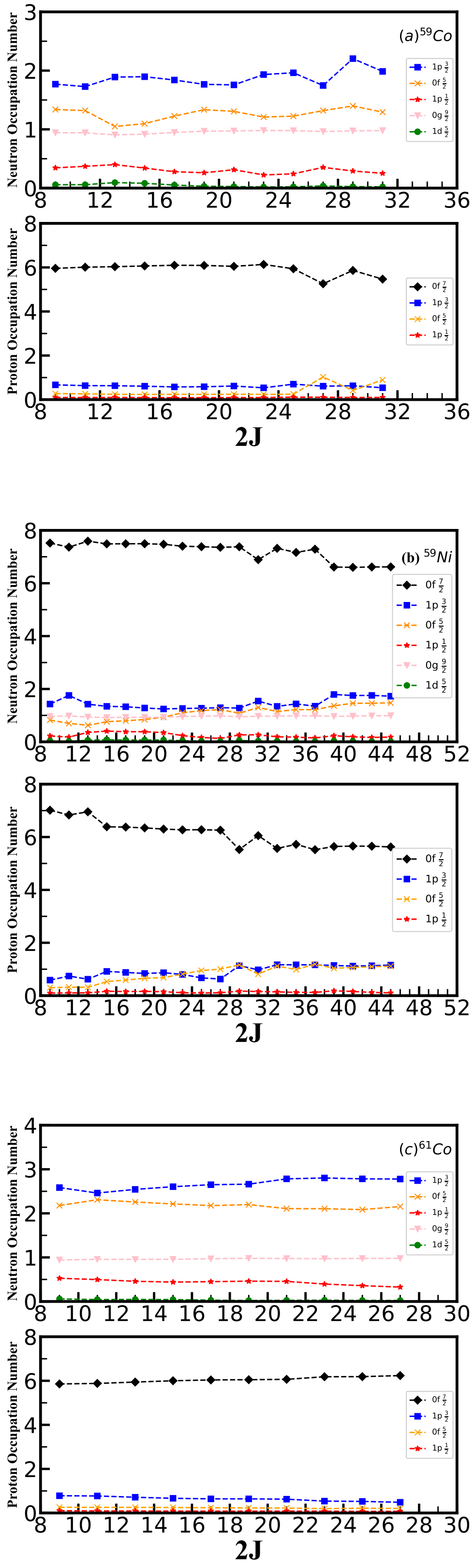

FIG. 15. Occupancy of the protons and neutrons in the positive parity state in (a) ^{59}Co (b) ^{59}Ni and (c) ^{61}Co as predicted by the shell model calculation. The orbitals are represented by different colors and shapes (blue box for $p_{3/2}$, orange X for $f_{5/2}$, red star for $p_{1/2}$, violet triangle for $g_{9/2}$, green circle for $d_{5/2}$ and black rhombus for $f_{7/2}$).

sitions observed for ^{61}Co, but one of the major bands has been reassigned as positive parity states by reason of this study.

It can be concluded from this study that the low-lying negative parity states in the three nuclei represent single particle excitations of the nucleons limited to the fp shell. The positive parity states and possibly the high-lying negative parity states in these nuclei are highly influenced by the presence of nucleons in the $g_{9/2}$ orbit. The presence of either strong $E2$ or $M1$ transitions observed in these nuclei suggests a form of collective excitation. We observe that collective excitation in ^{59}Co is dominated by magnetic rotation which can be explained by the shears mechanism. However, the collective excitations in ^{59}Ni and ^{61}Co are both in the form of magnetic rotation (though only tentative indications in ^{59}Ni) and rotations due to deformation. This implies that the excitation of neutrons into the $g_{9/2}$ orbit creates deformation in ^{59}Ni and ^{61}Co which in turn brings about a rotation that competes with the magnetic rotation occurring with little to no deformation. The three nuclei studied highlight the competition between single particle excitations and collective excitations in the excited states observed. The large scale shell model calculations presented here reproduced the excited states for the most part. However, the departures at the very high spins clearly point to the need for refinements of calculation to include more than one nucleon moving to the $g_{9/2}$ orbit.

VII. ACKNOWLEDGEMENT

This work was supported by the U.S. National Science Foundation under grant number Phy-2012522 (FSU) and the U.S. Department of Energy, office of Science, under award number DE-AC05-00OR22725 (ORNL). Noritaka Shimizu and Yutaka Utsuno acknowledge the support by ÁÁProgram for Promoting Researches on the Supercomputer Fugaku ©(JPMXP1020200105) and Multidisciplinary Cooperative Research Program, Tsukuba-CCS (wo22i002).

---

[1] C. Andreoiu, D. Rudolph, I. Ragnarsson, C. Fahlander, R. Austin, M. Carpenter, R. Clark, J. Ekman, R. Janssens, T. Khoo, F. Kondev, T. Lauritsen, T. Rodinger, D. Sarantites, D. Seweryniak, T. Steinhardt, C. Svensson, O. Thelen, and J. Waddington, Evolution of shapes in ^{59}Cu, The European Physical Journal A - Hadrons and Nuclei **14** (2002).

[2] Andersson, L. -L., Rudolph, D., Johansson, E. K., Torres, D. A., Carlsson, B. G., Ragnarsson, I., Andreoiu, C., Baktash, C., Carpenter, M. P., Charity, R. J., Chiara, C. J., Ekman, J., Fahlander, C., Hoel, C., Pechenaya, O. L., Reviol, W., du Rietz, R., Sarantites, D. G., Seweryniak, D., Sobotka, L. G., Yu, C. H., and Zhu, S., Extensive y spectroscopy of normally and superdeformed structures in $^{61}_{29}$Cu$_{32}$, Eur. Phys. J. A **36**, 251 (2008).

[3] D. Steppenbeck, A. N. Deacon, S. J. Freeman, R. V. F. Janssens, S. Zhu, M. P. Carpenter, P. Chowdhury, M. Honma, T. Lauritsen, C. J. Lister, D. Seweryniak, J. F. Smith, S. L. Tabor, and B. J. Varley, High-spin structures in the neutron-rich isotopes $^{57-60}$Mn, Phys. Rev. C **81**, 014305 (2010).

[4] A. M. Nathan, J. W. Olness, E. K. Warburton, and J. B. McGrory, Yrast decay schemes from heavy-ion + ^{48}Ca fusion-evaporation reactions. iii. ^{57,58}Fe, ^{54,55}Cr, and ^{57,58}Mn, Phys. Rev. C **17**, 1008 (1978).

[5] A. N. Deacon, S. J. Freeman, R. V. F. Janssens, M. Honma, M. P. Carpenter, P. Chowdhury, T. Lauritsen, C. J. Lister, D. Seweryniak, J. F. Smith, S. L. Tabor, B. J. Varley, F. R. Xu, and S. Zhu, Yrast structures in the neutron-rich isotopes ^{59,60}Fe and the role of the $g_{9/2}$ orbital, Phys. Rev. C **76**, 054303 (2007).

[6] A. D. Ayangeakaa, S. Zhu, R. V. F. Janssens, M. P. Carpenter, M. Albers, M. Alcorta, T. Baugher, P. F. Bertone, C. J. Chiara, P. Chowdhury, H. M. David, A. N. Deacon, B. DiGiovine, A. Gade, C. R. Hoffman, F. G. Kondev, T. Lauritsen, C. J. Lister, E. A. McCutchan, D. S. Moerland, C. Nair, A. M. Rogers, and D. Seweryniak, Role of the $\nu g_{9/2}$ orbital in the development of collectivity in the A $\approx$ 60 region: The case of ^{61}Co, Phys. Rev. C **91**, 044327 (2015).

[7] E. K. Johansson, D. Rudolph, I. Ragnarsson, L. L. Andersson, D. A. Torres, C. Andreoiu, C. Baktash, M. P. Carpenter, R. J. Charity, C. J. Chiara, J. Ekman, C. Fahlander, O. L. Pechenaya, W. Reviol, R. du Rietz, D. G. Sarantites, D. Seweryniak, L. G. Sobotka, C. H. Yu, and S. Zhu, Thorough γ-ray and particle decay investigations of ^{58}Ni, Phys. Rev. C **80**, 014321 (2009).

[8] R. Clark, R. Wadsworth, E. Paul, C. Beausang, I. Ali, A. Astier, D. Cullen, P. Dagnall, P. Fallon, M. Joyce, M. Meyer, N. Redon, P. Regan, W. Nazarewicz, and R. Wyss, First observation of a collective dipole rotational band in the A $\approx$ 200 mass region, Physics Letters B **275**, 247 (1992).

[9] G. Baldsiefen, U. Birkental, H. Hübel, N. Nenoff, B. Thirumala Rao, P. Willsau, J. Heese, H. Kluge, K. Maier, R. Schubart, and S. Frauendorf, First observation of a crossing of oblate dipole bands in the A $\approx$ 200 region, Physics Letters B **298**, 54 (1993).

[10] D. Steppenbeck, R. V. F. Janssens, S. J. Freeman, M. P. Carpenter, P. Chowdhury, A. N. Deacon, M. Honma, H. Jin, T. Lauritsen, C. J. Lister, J. Meng, J. Peng, D. Seweryniak, J. F. Smith, Y. Sun, S. L. Tabor, B. J. Varley, Y.-C. Yang, S. Q. Zhang, P. W. Zhao, and S. Zhu, Magnetic rotation and quasicollective structures in ^{58}fe: Influence of the $\nu g_{9/2}$ orbital, Phys. Rev. C **85**, 044316 (2012).

[11] N. Sensharma, A. D. Ayangeakaa, R. V. F. Janssens, Q. B. Chen, S. Zhu, M. Alcorta, M. P. Carpenter, E. A. McCutchan, F. G. Kondev, T. Lauritsen, D. Seweryniak, C. R. Hoffman, A. M. Rogers, A. Gade, T. Baugher, and P. Chowdhury, Single-particle and dipole excitations in ^{62}Co, Phys. Rev. C **105**, 044315 (2022).

[12] D. A. Torres, F. Cristancho, L.-L. Andersson, E. K. Johansson, D. Rudolph, C. Fahlander, J. Ekman, R. du Rietz, C. Andreoiu, M. P. Carpenter, D. Seweryniak, S. Zhu, R. J. Charity, C. J. Chiara, C. Hoel, O. L. Pechenaya, W. Reviol, D. G. Sarantites, L. G. Sobotka, C. Baktash, C.-H. Yu, B. G. Carlsson, and I. Ragnarsson, Deformations and magnetic rotations in the ^{60}Ni nucleus, Phys. Rev. C **78**, 054318 (2008).

[13] S. Bhattacharya, V. Tripathi, E. Rubino, S. Ajayi, L. T. Baby, C. Benetti, R. S. Lubna, S. L. Tabor, J. Döring, Y. Utsuno, N. Shimizu, J. M. Almond, and G. Mukherjee, Coexistence of single-particle and collective excitation in ^{61}Ni, Phys. Rev. C **107**, 054311 (2023).

[14] J. Lin, Y. K. Wang, C. Xu, Z. H. Li, H. Hua, S. Q. Zhang, D. W. Luo, H. Y. Wu, J. Meng, X. G. Wu, Y. Zheng, C. B. Li, T. X. Li, Z. Y. Huang, H. Cheng, C. Y. Guo, Z. X. Zhou, Z. Q. Chen, and C. G. Wang, Possible coexistence of magnetic and antimagnetic rotations in ^{61}Ni, Phys. Rev. C **107**, 014307 (2023).

[15] D. W. Luo, C. Xu, Y. K. Wang, Z. H. Li, R. A. Bark, S. Q. Zhang, H. Hua, S. Y. Wang, J. Peng, X. Q. Li, H. Y. Wu, X. Wang, C. G. Wu, Q. T. Li, J. Lin, Y. Jin, W. Z. Xu, L. Mu, J. Meng, F. R. Xu, Y. L. Ye, D. X. Jiang, P. Jones, E. A. Lawrie, P. Papka, M. F. Nkalanga, T. D. Bucher, M. V. Chisapi, L. Msebi, S. Jongile, S. Ntshangase, B. R. Zikhali, S. H. Mthembu, T. Seakamela, M. A. Sithole, O. Shirihda, A. A. Aava, L. Mdletshe, K. L. Malatji, S. Mhlongo, and L. Makhathini, Collective structures in ^{62}Cu, Phys. Rev. C **105**, 024305 (2022).

[16] P. Zhao, S. Zhang, J. Peng, H. Liang, P. Ring, and J. Meng, Novel structure for magnetic rotation bands in 60ni, Physics Letters B **699**, 181 (2011).

[17] W. Reviol, D. G. Sarantites, R. J. Charity, V. Tomov, J. Dobaczewski, D. Rudolph, R. M. Clark, M. Cromaz, P. Fallon, A. O. Macchiavelli, M. P. Carpenter, and D. Seweryniak, Highly deformed band structure in ^{57}Co, Phys. Rev. C **65**, 034309 (2002).

[18] J. Dobaczewski and P. Olbratowski, Solution of the skyrme–hartree–fock–bogolyubov equations in the cartesian deformed harmonic-oscillator basis. (iv) hfodd (v2.08i): a new version of the program, Computer Physics Communications **158**, 158 (2004).

[19] J. Meng, J. Peng, S.-Q. Zhang, and P.-W. Zhao, Progress on tilted axis cranking covariant density functional theory for nuclear magnetic and antimagnetic rotation, Frontiers of Physics **8**, 55 (2013).

[20] A. V. Afanasjev, I. Ragnarsson, and P. Ring, Comparative study of superdeformed and highly deformed bands in the $a \sim 60$ mass region, Phys. Rev. C **59**, 3166 (1999).

[21] R. Schwengner, G. Rainovski, H. Schnare, A. Wagner, F. Dönau, A. Jungclaus, M. Hausmann, O. Iordanov, K. P. Lieb, D. R. Napoli, G. de Angelis, M. Axiotis, N. Marginean, F. Brandolini, and C. Rossi Alvarez, Magnetic rotation in ^{82}Rb and ^{84}Rb, Phys. Rev. C **66**, 024310 (2002).

[22] C. Y. He, X. Q. Li, L. H. Zhu, X. G. Wu, B. Qi, Y. Liu, B. Pan, G. S. Li, L. H. Li, Z. M. Wang, Z. Y. Li, S. Y. Wang, Q. Xu, J. G. Wang, H. B. Ding, and J. Zhai, Magnetic rotation in ^{112}In, Phys. Rev. C **83**, 024309 (2011).

[23] H. Hübel, Magnetic rotation in nuclei, Progress in Particle and Nuclear Physics **54**, 1 (2005).

[24] R. M. Clark and A. O. Macchiavelli., The shears mechanism in nuclei, Annual Review of Nuclear and Particle Science **50**, 1 (2000).

[25] E. K. Warburton, J. W. Olness, A. M. Nathan, J. J. Kolata, and J. B. McGrory, Yrast decay schemes from heavy-ion + ^{48}Ca fusion-evaporation reactions. ii. $^{59-60}$Fe and $^{59-60}$Co, Phys. Rev. C **16** (1977).

[26] K. Coop, I. Graham, and E. Titterton, An investigation of ^{59}Co and ^{61}Co using the ^{56}Fe(α, pγ) and ^{64}Ni(p, $\alpha\gamma$) reactions, Nuclear Physics A **150**, 346 (1970).

[27] P. Haupt, J. W. Koen, W. J. Naude, and N. J. A. Rust, Properties of low-lying levels of ^{59}Co, Z.Phys. **A295**, 135 (1980).

[28] C.-H. Yu, C. Baktash, J. A. Cameron, M. Devlin, J. Eberth, A. Galindo-Uribarri, D. S. Haslip, D. R. LaFosse, T. J. Lampman, I.-Y. Lee, F. Lerma, A. O. Macchiavelli, S. D. Paul, D. C. Radford, I. Ragnarsson, D. Rudolph, D. G. Sarantites, C. E. Svensson, J. C. Waddington, J. C. Wells, and J. N. Wilson, Rotational bands with terminating properties in ^{59}Ni, Phys. Rev. C **65**, 061302(R) (2002).

[29] K. Krane, R. Steffen, and R. Wheeler, Directional correlations of gamma radiations emitted from nuclear states oriented by nuclear reactions or cryogenic methods, Atomic Data and Nuclear Data Tables **11**, 351 (1973).

[30] P. Jones, L. Wei, F. Beck, P. Butler, T. Byrski, G. Duchêne, G. de France, F. Hannachi, G. Jones, and B. Kharraja, Calibration of the new composite "clover" detector as a compton polarimeter for the eurogam array, Nuclear Instruments and Methods in Physics Research Section A: Accelerators, Spectrometers, Detectors and Associated Equipment **362**, 556 (1995).

[31] A. M. Nathan, J. W. Olness, E. K. Warburton, and J. B. McGrory, Yrast decay schemes from heavy ion + ^{48}Ca fusion-evaporation reactions. i. $^{54-56}$Mn, ^{56}Cr, and $^{52-53}$V, Phys. Rev. C **16**, 192 (1977).

[32] O. Tarasov and D. Bazin, Lise++: Radioactive beam production with in-flight separators, Nuclear Instruments and Methods in Physics Research Section B: Beam Interactions with Materials and Atoms **266**, 4657 (2008), proceedings of the XVth International Conference on Electromagnetic Isotope Separators and Techniques Related to their Applications.

[33] A. Gavron, Statistical model calculations in heavy ion reactions, Phys. Rev. C **21**, 230 (1980).

[34] S. Juutinen, J. Hattula, M. Jääskeläinen, A. Virtanen, and T. Lönnroth, Excited structure of the ^{56}Ni-plus-three-nucleon isobars ^{59}Ni and ^{59}Cu, Nuclear Physics A **504**, 205 (1989).

[35] N. Shimizu, T. Mizusaki, Y. Utsuno, and Y. Tsunoda, Thick-restart block lanczos method for large-scale shell-model calculations, Computer Physics Communications **244**, 372 (2019).

[36] T. Togashi, N. Shimizu, Y. Utsuno, T. Otsuka, and M. Honma, Large-scale shell-model calculations for unnatural-parity high-spin states in neutron-rich cr and fe isotopes, Phys. Rev. C **91**, 024320 (2015).

[37] J. N. Roy, H. M. S. Gupta, A. R. Majumder, T. Congedo, and J. E. Alzona, Level properties of ^{60}Co from the (d,p) reaction on ^{59}Co, Journal of Physics G: Nuclear Physics **4**, 1469 (1978).

[38] T. Bengtsson and I. Ragnarsson, Rotational bands and particle-hole excitations at very high spin, Nuclear Physics A **436**, 14 (1985).

[39] H. Sultana, R. Bhattacharjee, A. Chakraborty, M. A. Khan, S. S. Bhattacharjee, R. Chakrabarti, S. Das, U. Garg, S. S. Ghugre, R. Palit, R. Raut, S. Saha, S. Samanta, J. Sethi, A. K. Sinha, and T. Trivedi, Possible onset of multifaceted excitation modes in ^{29}Al, Phys. Rev. C **98**, 014330 (2018).

[40] P. H. Regan, J. W. Arrison, U. J. Hüttmeier, and D. P. Balamuth, Yrast γ-ray spectroscopy of the neutron rich isotopes ^{61,63}Co, Phys. Rev. C **54**, 1084 (1996).

[41] K. Zuber and B. Singh, Nuclear data sheets for A = 61, Nuclear Data Sheets **125**, 1 (2015).

Appendices

TABLE I: This table show the details of the γ transitions observed in the present work on ^{59}Co. The DCO ratio (R_{DCO}) was calculated for quadrupole transitions except for those with the D symbol which are from dipole transitions. The relative intensities, I_γ less than 6% are given to 1 decimal place.

Begin of Table								
E_i (keV)	E_f (keV)	E_γ (keV)	I_γ (%)	J_i^π	J_f^π	R_{DCO}	Asymmetry	Multipolarity
1190.7 (5)	0	1190.7 (5)	100 (11)	$9/2^-$	$7/2^-$	$0.91\ (6)^D$	-0.014 (10)	M1
1460.4 (5)	0	1460.4 (5)	100 (9)	$11/2^-$	$7/2^-$	$1.63\ (9)^D$	0.013 (13)	E2
	1190.7	269.2 (5)	13 (1)	$11/2^-$	$9/2^-$	$1.26\ (9)^D$		D
2154.9 (7)	1460.4	694.5 (5)	74 (7)	$13/2^-$	$11/2^-$	0.63 (5)	-0.0077 (11)	M1
2183.7 (8)	1190.7	993.0 (6)	77 (11)	$11/2^-$	$9/2^-$	$1.03\ (7)^D$		D
	0	2183.7 (8)	3.2 (3)	$11/2^-$	$7/2^-$			
2915.4(10)	2154.9	760.5 (7)	21 (2)	$15/2^-$	$13/2^-$	0.68 (5)	-0.0005 (9)	M1/E2
3083.4 (8)	1190.7	1892.7 (6)	5.2 (5)	$11/2^-$	$9/2^-$	$1.04\ (7)^D$	-0.057 (18)	M1
3224.9 (9)	2183.7	1041.2 (5)	5.0 (3)	$13/2^{(-)}$	$11/2^-$	$1.00\ (14)^D$		D
	1460.4	1764.9 (9)	6 (1)	$13/2^{(-)}$	$11/2^-$	$1.07\ (11)^D$		D
3627.5(11)	2915.4	712.1 (5)	16 (2)	$17/2^{(-)}$	$15/2^-$	0.62 (5)		D
3738.4(9)	2154.9	1583.5(5)	11 (1)	$15/2^-$	$13/2^-$	0.71 (5)	-0.0016 (10)	M1
3844.3(10)	1190.7	2653.6 (6)	12 (1)	$11/2^+$	$9/2^-$	$0.81\ (6)^D$	0.075 (21)	E1
	1460.4	2383.9 (9)	7 (1)	$11/2^+$	$11/2^-$	0.98 (7)	0.075 (14)	E2, $\Delta J = 0$
	2154.9	1690.2 (8)	4.9 (3)	$11/2^+$	$13/2^-$	$0.79\ (6)^D$		D
4178.7(11)	2183.7	1995.3 (5)	33 (2)	$13/2^+$	$11/2^-$	$0.97\ (7)^D$	0.066 (13)	E1
	3844.3	334.4 (5)	14 (1)	$13/2^+$	$11/2^+$	$0.97\ (7)^D$		D
	1460.4	2719.4 (5)	10 (1)	$13/2^+$	$11/2^-$	0.54 (5)	0.083 (22)	E1
	3083.4	1095.1 (5)	5.0 (4)	$13/2^+$	$11/2^-$	0.62 (5)		D
	2154.9	2025.3 (5)	4.5 (3)	$13/2^+$	$13/2^-$			$\Delta J = 0$
4414.6(11)	4178.7	235.9 (5)	41 (3)	$15/2^+$	$13/2^+$	$1.14\ (3)^D$		D
	2154.9	2260.6 (5)	17 (1)	$15/2^+$	$13/2^-$	0.48 (5)	0.055 (13)	E1
	3224.9	1190.3 (6)	4.8 (4)	$15/2^+$	$13/2^-$	$0.91\ (6)^D$		D
4489.6(9)	1460.4	3029.2 (8)	3.5 (2)	$15/2^{(-)}$	$11/2^-$	1.25 (18)		Q
4717.5(12)	4414.6	302.9 (5)	55 (7)	$17/2^+$	$15/2^+$	0.68 (5)		D
4785.2(13)	3738.4	1046.8 (9)	3.4 (3)	$17/2^{(-)}$	$15/2^-$	$1.23\ (9)^D$		D
4799.9(12)	3627.5	1172.4 (5)	13 (6)	$19/2^{(-)}$	$17/2^{(-)}$	0.67 (5)		D
5370.6(13)	4717.5	653.1 (5)	53 (5)	$19/2^+$	$17/2^+$	0.58 (4)	-0.017 (12)	M1
5444.8(11)	2154.9	3289.9 (9)	3.4 (3)	$17/2^{(-)}$	$13/2^-$	1.19 (13)		Q
5574.8(11)	2154.9	3419.9 (9)	3.4 (3)	$15/2^{(-)}$	$13/2^-$	0.48 (5)		D
6364.6(14)	5370.6	994.0 (6)	25 (4)	$21/2^+$	$19/2^+$	0.50 (5)		D
6422.4(13)	4799.9	1622.5 (5)	2.9 (3)	$19/2^{(-)}$	$19/2^{(-)}$	1.14 (8)		$\Delta J = 0$
	3627.5	2794.0 (7)	2.8 (2)	$19/2^{(-)}$	$17/2^{(-)}$	0.70 (8)		D
6878.7(14)	5370.6	1508.9 (5)	5.1 (5)	$21/2^{(-)}$	$19/2^+$	0.50 (5)		D
	4799.9	2078.8 (5)	10 (1)	$21/2^{(-)}$	$19/2^{(-)}$	0.54 (5)		D
	6422.4	457.1 (5)	4.1 (4)	$21/2^{(-)}$	$19/2^{(-)}$	0.68 (5)	-0.0035 (10)	M1
7459.7(15)	6364.6	1095.1 (5)	9 (1)	$23/2^+$	$21/2^+$	0.62 (5)	-0.020 (13)	M1
7842.7(15)	6364.6	1478.1 (5)	10 (1)	$23/2^{(+)}$	$21/2^+$	0.71 (5)		D
7903.9(15)	6364.6	1539.3 (5)	5.0 (4)	$23/2^{(-)}$	$21/2^+$	$1.16\ (8)^D$	0.013 (12)	E1
	6878.7	1025.6 (6)	5.0 (4)	$23/2^{(-)}$	$21/2^{(-)}$	0.64 (5)	-0.0080 (11)	M1
8118.5(16)	6878.7	1239.8(8)	3.7 (3)	$23/2^{(-)}$	$21/2^{(-)}$	0.73 (5)		D
8868.1 (16)	7903.9	964.2 (6)	3.9 (3)	$25/2^{(-)}$	$23/2^{(-)}$	0.66 (6)		D
8898.2(16)	7459.7	1437.6 (6)	5.0 (5)	$25/2^{(+)}$	$23/2^+$	0.41 (5)		D
9105.4(17)	7459.7	1644.8 (9)	3.5 (3)	$25/2^{(+)}$	$23/2^+$	$1.14\ (8)^D$		D
9343.8(15)	6364.6	2979.2 (5)	3.6 (3)	$25/2^{(+)}$	$21/2^+$	$2.08\ (23)^D$	0.027 (15)	E2
9552.9(16)	7903.9	1649.0 (5)	3.9 (2)	$27/2^{(-)}$	$23/2^{(-)}$	1.06 (11)		Q
9815.1(16)	7842.7	1971.5 (5)	4.1 (4)	$27/2^{(+)}$	$23/2^{(+)}$	0.94 (7)	0.21 (4)	E2
10073.2(16)	9343.8	729.4 (5)	3.2 (5)	$27/2^{(+)}$	$25/2^{(+)}$	0.68 (5)		D
10091.0(16)	7459.7	2630.4 (6)	2.9 (2)	$27/2^{(+)}$	$23/2^+$	1.13 (13)	0.12 (5)	E2

Continuation of Table I

E_i (keV)	E_f (keV)	E_γ (keV)	I_γ (%)	J_i^π	J_f^π	R_{DCO}	Asymmetry	Multipolarity
10888.7(17)	10091.0	795.7 (7)	2.7 (4)	$31/2^{(+)}$	$27/2^{(+)}$	1.25 (8)		Q
11140.1(18)	9815.1	1325.0 (8)	3.5 (5)	$31/2^{(+)}$	$27/2^{(+)}$	1.64 (12)^D		Q

End of Table

TABLE II: This table show the details of the γ transitions observed in the present work on ^{59}Ni. The R_{DCO} was calculated for quadrupole transitions except for those with the D symbol which are from dipole transitions. The relative intensities, I_γ less than 6% are given to 1 decimal place.

Begin of Table

E_i (keV)	E_f (keV)	E_γ (keV)	I_γ (%)	J_i^π	J_f^π	R_{DCO}	Asymmetry	Multipolarity
339.5(5)	0	339.5(5)	100 (10)	$5/2^-$	$3/2^-$	0.74 (5)		D
1189.0(5)	0	1189.0(5)*	53 (16)	$5/2^-$	$3/2^-$	0.52 (6)		D
1339.0(6)	339.5	998.0(5)*	61 (15)	$7/2^-$	$5/2^-$	0.96 (6)^D		D
	0	1339.0(6)	39 (7)	$7/2^-$	$3/2^-$	1.67 (16)^D	0.053 (11)	E2
1768.5(7)	339.5	1429.0(5)	63 (9)	$9/2^-$	$5/2^-$	0.93 (13)	0.093 (13)	E2
	1339.0	429.1(8)	18 (2)	$9/2^-$	$7/2^-$	0.87 (9)^D		D
1949.7(7)	0	1949.7(7)	16 (3)	$7/2^-$	$3/2^-$	0.94 (7)	0.079 (13)	E2
	339.5	1610.4(5)	9 (4)	$7/2^-$	$5/2^-$	0.58 (4)		D
	1189.0	759.0(5)	6 (1)	$7/2^-$	$5/2^-$	0.56 (7)		D
	1339.0	610.0 (5)	4.4 (2)	$7/2^-$	$7/2^-$	1.79 (17)^D		$\Delta J = 0$
2530.0(8)	1339.0	1191.0(5)	6 (1)	$9/2^-$	$7/2^-$	0.90 (9)^D		D
	339.5	2193.0(6)	2.1 (3)	$9/2^-$	$5/2^-$	1.74 (17)^D		Q
2707.0(7)	1339.0	1368.0(5)	58 (4)	$11/2^-$	$7/2^-$	1.50 (14)^D	0.13 (1)	E2
	1768.5	938.3(5)	15 (1)	$11/2^-$	$9/2^-$	0.42 (3)		D
3056.6(7)	1949.7	1105.9(8)	26 (4)	$9/2^+$	$7/2^-$	0.57 (4)	0.086 (12)	E1
	1339.0	1717.6(5)	9 (2)	$9/2^+$	$7/2^-$	0.59 (4)	0.040 (12)	E1
3126.5(9)	1768.5	1358.0(6)	3.3 (3)	$11/2^-$	$9/2^-$	0.88 (11)^D		D
	339.5	2783.0(7)	2.1 (4)	$11/2^-$	$5/2^-$			
3378.2(9)	1768.5	1609.7(5)	24 (1)	$11/2^-$	$9/2^-$	0.66 (7)		D
	2707.0	674.0(5)	22 (3)	$11/2^-$	$11/2^-$	0.89 (9)		$\Delta J = 0$
3561.8(8)	1768.5	1793.3 (5)	24 (4)	$11/2^-$	$9/2^-$	0.71 (5)	-0.0040 (11)	M1
	2707.0	854.6(8)	22 (3)	$11/2^-$	$11/2^-$			$\Delta J = 0$
	2530.0	1029.0(5)	6 (3)	$11/2^-$	$9/2^-$	1.09 (11)^D		D
	3126.5	433.6(5)	5.0 (6)	$11/2^-$	$11/2^-$	1.27 (13)		$\Delta J = 0$
	1949.7	1612.0(5)	5.0 (5)	$11/2^-$	$7/2^-$			
	1339.0	2223.2(6)	3.8 (3)	$11/2^-$	$7/2^-$	1.07 (8)		Q
4104.7(9)	1768.5	2336.2(5)	6 (1)	$11/2^+$	$9/2^-$	0.76 (5)	0.062 (19)	E1
4143.8(9)	3378.2	764.9(5)	31 (2)	$13/2^-$	$11/2^-$	0.99 (8)^D	-0.0005 (9)	M1
	3561.8	582.0(5)	27 (2)	$13/2^-$	$11/2^-$	0.90 (9)^D	-0.033 (9)	M1
	2707.0	1435.0(5)	2.2 (3)	$13/2^-$	$11/2^-$			
4419.0(10)	1768.5	2650.5(8)	6 (1)	$13/2^-$	$9/2^-$	1.15 (10)	0.058 (18)	E2
	3561.8	858.0(8)	2.7 (2)	$13/2^-$	$11/2^-$			
4457.8(9)	3056.6	1401.5(5)	25 (2)	$13/2^+$	$9/2^+$	0.82 (6)	0.069 (12)	E2
	2707.0	1750.8(5)	24 (2)	$13/2^+$	$11/2^-$	0.44 (6)	0.054 (12)	E1
4727.2(9)	1768.5	2958.7(5)	3.1 (3)	$11/2^+$	$9/2^-$	0.56 (8)	0.030 (14)	E1
4910.7(10)	1768.5	3142.2(7)	4.4 (3)	$11/2^+$	$9/2^-$	0.64 (9)	0.070 (24)	E1
4950.5(10)	4143.8	806.7(5)	29 (4)	$15/2^-$	$13/2^-$	0.87 (9)^D	-0.055 (12)	M1
	3378.2	1571.0(6)	3.1 (2)	$15/2^-$	$11/2^-$			
5100.0(9)	3561.8	1539.0(7)	3.7 (2)	$13/2^{(-)}$	$11/2^-$	1.27 (13)^D		D
	2707.0	2393.0(6)	2.3 (2)	$13/2^-$	$11/2^-$			
5254.6(10)	4457.8	796.8(5)	32 (2)	$17/2^+$	$13/2^+$	1.00 (7)	0.051 (25)	E2
	4950.5	303.0(5)	2.9 (1)	$17/2^+$	$15/2^-$	1.08 (11)^D		D
5295.0(11)	4143.8	1151.2(7)	4.5 (3)	$15/2^-$	$13/2^-$	0.78 (8)^D	-0.025 (14)	M1
5383.2(10)	4143.8	1239.4(6)	10 (1)	$15/2^+$	$13/2^-$	1.29 (13)^D	0.10 (1)	E1
	4104.7	1279.3(5)	4.4 (4)	$15/2^+$	$11/2^+$	1.08 (8)		Q
5947.7(11)	4950.5	997.2(5)	16 (4)	$17/2^{(-)}$	$15/2^-$	0.94 (7)^D		D
5991.8(11)	4457.8	1534.0(6)	5.0 (5)	$17/2^+$	$13/2^+$			

Continuation of Table II

E_i (keV)	E_f (keV)	E_γ (keV)	I_γ (%)	J_i^π	J_f^π	R_{DCO}	Asymmetry	Multipolarity
6079.3(10)	4143.8	1935.5(5)	14 (2)	$17/2^-$	$13/2^-$	0.98 (7)	0.069 (20)	E2
6483.8(12)	5947.7	536.1(6)	5.0 (4)	$19/2^{(-)}$	$17/2^{(-)}$	0.57 (4)	-0.0017 (99)	M1
6505.6(12)	6079.3	426.6(5)	11 (2)	$19/2^-$	$17/2^-$	0.70 (5)		D
	4950.5	1555.1(7)	10 (1)	$19/2^-$	$15/2^-$	1.32 (9)	0.037 (11)	E2
6749.6(10)	5100.0	1649.6(5)	3.1 (2)	$15/2^{(-)}$	$13/2^{(-)}$	$0.87\ (9)^D$		D
7167.5(13)	6505.6	661.9(5)	17 (2)	$21/2^{(-)}$	$19/2^-$	0.71 (5)		D
	5254.6	1912(9)	2.1 (1)	$21/2^-$	$17/2^+$			
7232.7(10)	6483.8	748.9(6)	4.3 (4)	$21/2^{(-)}$	$19/2^{(-)}$	0.7 (1)		D
7393.7(13)	5254.6	2139.1(8)	5.5 (4)	$19/2^-$	$17/2^+$	0.75 (6)	0.021 (11)	E1
7636.8(13)	6505.6	1131.2(5)	3.0 (2)	$21/2^{(-)}$	$19/2^-$	$0.87\ (10)^D$		D
7954.2(14)	7167.5	786.7(5)	11 (1)	$23/2^{(-)}$	$21/2^{(-)}$	0.48 (5)	-0.024 (11)	M1
8132.8(13)	5254.6	2878.2(7)	14 (1)	$21/2^+$	$17/2^+$	1.16 (10)	0.052 (13)	E2
8290.7(14)	7393.7	897.0(5)	4.9 (2)	$23/2^-$	$19/2^-$	0.95 (7)	0.011 (11)	E2
8632.3(15)	7954.2	678.1(5)	10 (3)	$25/2^{(-)}$	$23/2^{(-)}$	0.58 (4)		D
9166.5(15)	8290.7	875.8(6)	4.2 (4)	$27/2$	$23/2^-$	1.12 (7)		Q
9309.7(16)	8632.3	677.4(5)	10 (2)	$27/2^{(-)}$	$25/2^{(-)}$	0.58 (4)		D
9753.4(16)	8632.3	1121.1(5)	2.1 (1)	$27/2^{(-)}$	$25/2^{(-)}$	$1.14\ (14)^D$	-0.12 (2)	M1
9901.5(14)	8132.8	1768.7(5)	7 (1)	$25/2^+$	$21/2^+$	1.08 (8)	0.084 (12)	E2
10089.1(17)	9309.7	779.4(5)	5.0 (4)	$29/2^{(-)}$	$27/2^{(-)}$	0.63 (7)		D
10421.8(14)	8132.8	2289.0(5)	4.7 (2)	$25/2^+$	$21/2^+$	1.26 (18)	0.072 (20)	E2
11645.0(15)	9901.5	1747.0(5)	3.8 (1)	$29/2^+$	$25/2^+$	$1.61\ (23)^D$		Q
	10421.8	1223.2 (5)	3.7 (1)	$29/2^+$	$25/2^+$	$1.58\ (16)^D$	0.047 (11)	E2
11911.8(16)	9901.5	2010.3(8)	3.7 (4)	$29/2^+$	$25/2^+$	1.00 (7)	0.11 (2)	E2
12007.5(18)	10089.1	1918.4(8)	2.5 (5)	$31/2^{(-)}$	$29/2^{(-)}$	$0.96\ (14)^D$		D
13229.0(17)	11645.0	1584.0(7)	5.2 (3)	$33/2^{(+)}$	$29/2^+$	$1.77\ (22)^D$		Q
14284.1(17)	11911.8	2372.3(6)	3.3 (3)	$33/2^{(+)}$	$29/2^+$	1.08 (10)		Q
15178.7(18)	13229.0	1949.7(7)	4.0 (5)	$37/2^{(+)}$	$33/2^{(+)}$	0.94 (7)	0.079 (13)	E2
16467.6(19)	14284.1	2183.5(9)	1.6 (7)	$(37/2^+)$	$33/2^+$			
17684.6(19)	15178.7	2505.9(5)	3.1 (3)	$41/2^{(+)}$	$37/2^{(+)}$			

End of Table

*The intensity measurement of the 1189.0- and 998.0-keV transition is complicated by nearby contaminant transitions.

TABLE III: This table show the details of the γ transitions observed in the present work on ^{61}Co. The R_{DCO} was calculated for quadrupole transitions except for those with the D symbol which are from dipole transitions. The relative intensities, I_γ less than 6% are given to 1 decimal place.

Begin of Table

E_i (keV)	E_f (keV)	E_γ (keV)	I_γ (%)	J_i^π	J_f^π	R_{DCO}	Asymmetry	Multipolarity
1285.9(5)	0	1285.9(5)	80 (8)	$9/2^-$	$7/2^-$	$1.11\ (11)^D$		D
1664.8(5)	0	1664.8(5)	100 (12)	$11/2^-$	$7/2^-$	$2.16\ (25)^D$	0.075 (12)	E2
	1285.9	378.4(5)	15 (1)	$11/2^-$	$9/2^-$	0.54 (8)		D
2339.4 (8)	1285.9	1053.5(6)	20 (2)	$11/2^-$	$9/2^-$	0.60 (6)		D
2374.4 (8)	1664.8	709.6(6)	35 (6)	$13/2^-$	$11/2^-$	0.66 (5)	-0.036 (11)	M1
3127.0 (9)	2374.4	752.6(5)	25 (7)	$15/2^-$	$13/2^-$	0.66 (7)	-0.041 (11)	M1
	1664.8	1462.0(6)	14 (4)	$15/2^-$	$11/2^-$	1.19 (12)		Q
3159.4(9)	1664.8	1494.6(8)	14 (1)	$13/2^-$	$11/2^-$	0.65 (6)		D
3472.5(7)	1664.8	1807.7(5)	42 (4)	$13/2^+$	$11/2^-$	0.59 (6)	0.030 (11)	E1
	2339.4	1131.6(6)	8 (2)	$13/2^+$	$11/2^-$	$0.81\ (8)^D$	0.044 (11)	E1
	2374.4	1097.6(9)	3.5 (5)	$13/2^+$	$13/2^-$			$\Delta J = 0$
3658.8(9)	3472.5	186.3(5)	35 (5)	$15/2^+$	$13/2^+$	0.55 (4)		D
	3127.0	531.2(5)	15 (4)	$15/2^+$	$15/2^-$	0.84 (8)		$\Delta J = 0$
3910.8(7)	1664.8	2246.0(5)	4.5 (2)	$13/2^-$	$11/2^-$			
4094.4(10)	3658.8	435.6(5)	28 (6)	$17/2^+$	$15/2^+$	0.68 (6)	-0.047 (11)	M1
	3127.0	966.6(6)	6 (1)	$17/2^+$	$15/2^-$	$0.99\ (10)^D$		D

Continuation of Table III

E_i (keV)	E_f (keV)	E_γ (keV)	I_γ (%)	J_i^π	J_f^π	R_{DCO}	Asymmetry	Multipolarity
4117.9(11)	3159.4	956.5(7)	12 (2)	$15/2^-$	$13/2^-$			
	2374.4	1743.5(8)	5 (1)	$15/2^-$	$13/2^-$	0.40 (5)		D
	3910.8	208.2(6)	4.9 (2)	$15/2^-$	$13/2^-$	0.66 (6)		D
	3658.8	456.5(7)	4.5 (6)	$15/2^-$	$15/2^+$		0.108 (13)	$\Delta J = 0$
4388.3(13)	4117.9	270.4(7)	12 (1)	$17/2^-$	$15/2^-$	0.44 (4)		D
	3658.8	728.3(7)	12 (4)	$17/2^-$	$15/2^+$	0.56 (6)		D
4485.4(8)	3472.5	1012.9(3)	12 (1)	$15/2^-$	$13/2^+$	0.72 (8)	0.107 (13)	E1
	3127.0	1358.4(6)	8 (1)	$15/2^-$	$15/2^-$	1.28 (11)^D		$\Delta J = 0$
4803.6(12)	4094.4	709.2(6)	27 (7)	$19/2^+$	$17/2^+$	0.66 (5)	-0.036 (11)	M1
4871.2(10)	4485.4	385.8(6)	19 (4)	$17/2^-$	$15/2^-$	0.64 (8)		D
	3658.8	1212.4(6)	5.0 (5)	$17/2^-$	$15/2^+$	0.87 (12)^D		D
5118.8(15)	4388.3	730.5(7)	6 (1)	$19/2^-$	$17/2^-$	0.56 (6)		D
5347.8(12)	4871.2	476.6(6)	5.0 (5)	$19/2^-$	$17/2^-$	0.97 (14) ^{D}		D
5723.3(13)	3658.8	2064.5(9)	7 (2)	$17/2^-$	$15/2^+$			
5814.3(11)	3658.8	2155.5(6)	3.4 (1)	$17/2^-$	$15/2^+$	0.38 (5)		D
5833.1(13)	4803.6	1029.5(6)	19 (1)	$21/2^+$	$19/2^+$	0.73 (7)		D
5955.8(17)	5347.8	608.5(5)	4.3 (4)	$21/2^-$	$19/2^-$	0.65 (6)		D
	5118.8	837.0(8)	3.8 (2)	$21/2^-$	$19/2^-$			
6066.6(17)	5118.8	947.8(8)	2.2 (4)	$21/2^-$	$19/2^-$	0.83 (7)^D		D
6170.5(12)	4094.4	2076.1(6)	10 (1)	$19/2^-$	$17/2^+$	0.67 (9)	0.045 (11)	E1
	5723.3	445.3(5)	7 (1)	$19/2^-$	$17/2^-$			
6710.4(13)	6170.5	539.9(6)	5.0 (3)	$21/2^-$	$19/2^-$	1.26 (18)^D		D
	5955.8	754.0(9)	4.1 (3)	$21/2^-$	$21/2^-$			$\Delta J = 0$
6749.2(18)	5955.8	793.4(7)	3.4 (5)	$23/2^-$	$21/2^-$			
6823(13)	6170.5	652.5(6)	5.0 (5)	$21/2^-$	$19/2^-$	0.51 (10)		D
	5814.3	1007.9(11)	3.2 (2)	$21/2^-$	$17/2^-$	0.96 (10)		Q
6894.9(14)	5833.1	1061.8(6)	7 (1)	$23/2^+$	$21/2^+$	0.50 (7)		D
7506.6(15)	6710.4	796.2(7)	4.5 (2)	$23/2^-$	$21/2^-$	0.61 (6)		D
7703.2(19)	6749.2	954.0(7)	2.8 (5)	$25/2^-$	$23/2^-$			
8089.5(14)	6823	1266.5(6)	3.2 (1)	$25/2^-$	$21/2^-$	0.93 (9)	0.099 (13)	E2
8216.7(16)	6894.9	1321.8(8)	4.3 (2)	$25/2^+$	$23/2^+$			
8408.1(16)	7506.6	901.5(6)	2.3 (2)	$25/2^-$	$23/2^-$			
9678.3(17)	8216.7	1461.6(7)	3.8 (3)	$27/2^+$	$25/2^+$			

End of Table

TABLE IV: A table showing the comparison between the energy levels from the experiment and the theoretical predictions from the shell model in ^{59}Co, ^{59}Ni, and ^{61}Co. Energy levels (experiment and theory) and differences are given in keV. 2J values in parenthesis are the states with tentative assignments of parity. 2J values with "*" indicate the second excited states (yrare states).

Begin of Table

Negative Parity States				Positive Parity States			
2J	Experiment	Theory	Difference	2J	Experiment	Theory	Difference
^{59}Co							
7	0	0	0	7	-	-	-
9	1191	1342	151	9	-	4314	-
11	1460	1494	34	11	3844	4497	653
13	2155	2178	23	13	4179	4773	594
15	2915	3251	336	15	4415	4783	368
(17)	3628	4756	1128	17	4718	5000	282
(19)	4800	5790	990	19	5371	5601	230
(21)	6879	6936	57	21	6366	6614	248
(23)	7904	8337	433	23	7460	7523	63
(25)	8868	9417	548	(25)	8898	8899	1
(27)	9553	10506	953	(27)	9815	9754	61
29	-	12338	-	29	-	11105	-
31	-	13601	-	(31)	10889	12061	1172
11*	2184	2158	26				

Continuation of Table IV							
Negative Parity States				Positive Parity States			
2J	Experiment	Theory	Difference	2J	Experiment	Theory	Difference
(13)*	3225	3208	17				
15*	3738	4019	281				
(17)*	4785	4919	134				
(19)*	6422	6098	324				
21*	-	7347	-				
(23)*	8119	8461	342				
25*	-	9836	-				
27*	-	11049	-				
29*	-	12469	-				
31*	-	13911	-				
^{59}Ni							
3	0	0	0	9	3057	3267	210
5	340	224	116	11	4105	4803	698
7	1339	1189	150	13	4458	4653	195
9	1769	1699	70	15	5383	6050	667
11	2707	2587	120	17	5255	5401	146
13	4144	3633	511	19	-	7139	-
15	4951	4469	482	21	8133	7875	258
(17)	5948	5380	568	23	-	8471	-
(19)	6484	6238	246	25	9902	9129	773
(21)	7168	7186	18	27	-	10161	-
(23)	7954	8361	407	29	11645	11593	52
(25)	8632	9656	1024	31	-	13111	-
(27)	9310	11391	2081	(33)	13229	13893	664
(29)	10089	12951	2862	35	-	15946	-
(31)	12008	14494	2486	(37)	15179	17047	1868
3*	-	966	-	39	-	18882	-
5*	1189	1527	338	(41)	17685	20283	2598
7*	1950	1749	201	43	-	21757	-
9*	2530	2652	122	45	-	23491	-
11*	3127	2883	244				
13*	4419	4010	409				
15*	5295	4735	560				
17*	6079	5654	425				
19*	6506	6419	87				
(21)*	7233	7999	766				
23*	8291	9321	1030				
25*	-	10587	-				
(27)*	9753	11973	2220				
29*	-	13211	-				
31*	-	14973	-				
^{61}Co							
7	0	0	0	7	-	-	-
9	1286	1536	250	9	-	3376	-
11	1665	1608	57	11	-	3432	-
13	2374	2259	115	13	3472	3411	61
15	3127	2939	188	15	3657	3577	80
17	4388	4833	445	17	4093	4054	39
19	5119	5898	779	19	4803	4932	129
21	5956	7349	1393	21	5832	5940	108
23	6749	7652	903	23	6893	6915	22
25	7703	8652	749	25	8135	8140	5
7*	-	1578	-	27	9597	9330	267
9*	-	2240	-				
11*	2339	2447	108				
13*	3159	3138	21				
15*	4118	3747	371				
17*	4871	5097	226				
19*	5348	5898	550				
21*	6067	7685	1618				

Continuation of Table IV							
Negative Parity States				Positive Parity States			
2J	Experiment	Theory	Difference	2J	Experiment	Theory	Difference
23*	7506	8242	736				
25*	8090	-	-				
End of Table							